Microfluidics-free single-cell genomics with templated emulsification

Iain C. Clark[1], Kristina M. Fontanez[2], Robert H. Meltzer[2], Yi Xue[2], Corey Hayford[2], Aaron May-Zhang[2], Chris D'Amato[2], Ahmad Osman[2], Jesse Q. Zhang[2], Pabodha Hettige[2], Cyrille L. Delley[3], Daniel W. Weisgerber[3], Joseph M. Replogle[4], Marco Jost[4,5], Kiet T. Phong[6], Vanessa E. Kennedy[7], Cheryl A. C. Peretz[8], Esther A. Kim[9], Siyou Song[9], William Karlon[10], Jonathan S. Weissman[4,11], Catherine C. Smith[7], Zev J. Gartner[6,12], Adam R. Abate[3,*]

[1]Department of Bioengineering, University of California, Berkeley, California Institute for Quantitative Biosciences, Berkeley, California, USA.

[2]Fluent Biosciences, Watertown, MA, USA.

[3]Department of Bioengineering and Therapeutic Sciences, University of California, San Francisco, San Francisco, California, USA.

[4]Whitehead Institute for Biomedical Research, Massachusetts Institute of Technology; Cambridge, MA, USA.

[5]Present address: Department of Microbiology, Harvard Medical School, Boston, Massachusetts, USA.

[6]Department of Pharmaceutical Chemistry, University of California San Francisco, San Francisco, CA, USA.

[7]Department of Medicine, University of California San Francisco, San Francisco, CA, USA.

[8]Department of Pediatrics, University of California San Francisco, San Francisco, CA, USA.

[9]Division of Plastic and Reconstructive Surgery, University of California San Francisco, San Francisco, CA, USA.

[10]Departments of Pathology and Laboratory Medicine, University of California San Francisco, San Francisco, CA, USA.

[11]Howard Hughes Medical Institute, Massachusetts Institute of Technology, Cambridge, MA 02142, USA.

[12]Chan Zuckerberg Biohub, San Francisco, CA, USA.

[*]Corresponding author: Adam R. Abate, adam@abatelab.org

Abstract

Single-cell RNA sequencing is now a standard method used to reveal the molecular details of cellular heterogeneity, but current approaches have limitations on speed, scale, and ease of use that stem from the complex microfluidic devices or fluid handling steps required for sample processing. We therefore developed a method that does not require specialized microfluidic devices, expertise, or hardware. Our approach is based on pre-templated instant partitions (PIPs) that allow single cell encapsulation and barcoding of cDNA in uniform droplet emulsions with only a vortexer. PIP-seq accommodates a wide range of emulsification formats, including microwell plates and large-volume conical tubes, enabling thousands of samples or millions of cells to be processed in minutes. We demonstrate that PIP-seq produces high-purity transcriptomes in mouse-human mixing studies, is compatible with multi-omics measurements, and can accurately characterize cell types in human breast tissue when compared to a commercial microfluidic platform. Single-cell transcriptional profiling of mixed phenotype acute leukemia using PIP-seq revealed the emergence of heterogeneity within chemotherapy resistant cell subsets that was hidden by standard immunophenotyping. PIP-seq is a simple, flexible, and scalable next generation workflow that extends single-cell sequencing to new applications, including screening, diagnostics, and disease monitoring.

Introduction

Single-cell RNA sequencing (scRNA-seq) is an essential technology in the biological sciences because it reveals how the properties of tissues arise from the transcriptional states of numerous interacting cells. Defining the gene expression signatures of individual cells allows cell type classification, the discovery of unique cell states during development and disease, and the prediction of regulatory mechanisms that control these states. As a result, bulk sequencing is being rapidly replaced by single-cell methods. The first single cell approaches isolated cells and prepared them individually for sequencing[1-4]. While improvements in molecular biology increased data quality[5,6], the requisite isolation and processing of separate cells ultimately limited throughput. Implementation of valve-based microfluidics reduced hands-on time[7], but failed to significantly increase cell number, and thus could not capture the heterogeneity intrinsic to most tissues. Advances in high throughput droplet microfluidic barcoding has expanded single-cell sequencing to tens of thousands of cells[8,9] and fueled biological discovery, but requires expensive instruments located in core facilities and therefore remains inaccessible to many labs. Methods for direct combinatorial indexing of cells[10,11], the use of nanowell arrays [12], or sample multiplexing[13,14] have overcome some limitations of microfluidics, but no current method simultaneously accommodates both low (10) and high ($>10^6$) cell numbers, can be applied to hundreds of independent samples, and can be rapidly implemented without custom equipment.

The scalability of single-cell methods is important for many applications, including tissue atlas projects[15-18], million cell perturbation experiments[19], drug development pipelines[20], and developmental studies[21]. Droplet microfluidics has an intrinsic disadvantage at high cell numbers due to the upper limit on drop generation speed. At high fluid velocities, droplet generation becomes uncontrolled, resulting in polydispersed emulsions and poor bead loading that reduces

single-cell data quality[22,23]. Therefore, to sequence millions of cells requires long run times, parallel droplet generators with complex designs that are prone to clogging, or implementation of additional barcoding steps prior to encapsulation[24]. More generally, droplet microfluidics relies on an expensive instrument usually located in a core facility, which necessitates sample transport or fixation that can alter RNA profiles. Centralized processing also reduces access to many labs and does not fit experiments that need rapid or point-of-collection sample handling, like remote field work or studies using infectious samples requiring biosafety precautions[12,25].

Much effort has thus gone into developing microfluidic-free single-cell methods. Split-pool ligation[10,11] and tagmentation[26,27] perform direct combinatorial barcoding of bulk suspensions, and significantly increase cell number; however, these laborious workflows require enormous numbers of pipetting operations and are poorly suited for low cell inputs. Moreover, while scalable, these methods require substantial expertise[28], and broad adoption of split-pool barcoding will likely require robotic automation in a centralized facility. Alternatively, methods based on nanowells prioritize simplicity and cost-effectiveness[12,25]. No microfluidics are required and wells are loaded by sedimentation, providing an instrument-free and point-of-use solution. However, nanowell array chips do not efficiently scale in cell or sample number; the planar arrays capture cells on a 2D surface and, thus, cannot compete with emulsions or combinatorial indexing utilizing a 3D volume that easily scales to millions of cells. Moreover, unless combined with multiplexing[13,14], nanowell chips are poorly suited for processing many separate samples because they require one array per sample, and thus hundreds of arrays for hundreds of samples. To advance the field of single-cell genomics, next generation technologies must simultaneously innovate on speed, scale, and ease of use. An ideal system would be compatible with barcoding of separate samples in well plates, accommodate orders-of-magnitude differences in cell number,

be completed in minutes, and be easy to conduct at the bench or in the field without specialized instrumentation. An approach that achieved these innovations simultaneously would significantly enhance the usefulness of single-cell genomics, impact basic and clinical research, and facilitate new diagnostics.

Here we describe PIP-seq, a flexible, scalable, and instrument-free scRNA-seq method based on pre-templated instant partitions (PIPs). The core of this approach is use of templated emulsification to encapsulate cells in droplets without microfluidics[29]. In contrast to microfluidic emulsification, in which droplets are created sequentially and thus their number scales with instrument run time, templated emulsification generates monodispersed droplets in parallel by bulk self-assembly and thus the number of droplets (and cells that can be barcoded) scales only with container volume. The result is an extremely scalable, user-friendly scRNA-seq method. PIP emulsions are equivalent to those generated with microfluidics and compatible with the latest innovations in multi-omic measurements. Here, we show that PIP-seq generates accurate gene expression profiles from human tissues and is compatible with multi-modal measurements of RNA and sgRNA (CROP-seq), or RNA and protein (CITE-seq). Finally, we demonstrate use of PIP-seq to monitor the response of patients with mixed phenotype acute leukemia (MPAL) to chemotherapy, revealing heterogeneity within cells with similar immunophenotypes. In summary, PIP-seq fills an unmet technical need by improving the speed, scalability, and ease-of-use of single-cell sequencing.

Results

Overview of the technology

PIP-seq uses particle templating to compartmentalize cells, barcoded beads, and lysis reagents in monodispersed water-in-oil droplets (**Fig. 1a**). Rapid emulsification with a standard vortexer

allows cells to be encapsulated at the bench or point of collection in minutes. The cells are lysed by increasing temperature to 65°C, which activates Proteinase K, releasing cellular mRNA that is captured on polyacrylamide beads decorated with barcoded polyA sequences (**Fig. 1b**). PIP-seq emulsions can be stored for days at 0°C without change in data quality **(Extended data Fig. 1)**, allowing samples to be banked for future processing. Upon resuming, oil is removed, beads are transferred into reverse transcription buffer, and full-length cDNA is synthesized, amplified, and prepared for sequencing (**Fig. 1c-d**).

A unique and valuable feature of PIP-seq is that cell encapsulation in droplets is performed in parallel using bead size to control droplet volume. In contrast to microfluidics, the number of droplets scales with total container volume, not emulsification time. For example, at a 6% collision rate that includes cell doublets and barcode reuse, we estimate that 3.5k cells can be barcoded with 35 µL of PIPs in a 500 µL tube, 225k cells can be barcoded with 2 mL of PIPs in a 15mL conical tube, and 1M cells can be barcoded with 10mL of PIPs in a 50mL conical tube. In all cases, only approximately two minutes of time is required (**Fig. 1e**). PIP-seq is equally scalable to large sample numbers. Encapsulation can be performed directly in 96, 384, or 1536 well plates (**Fig. 1f**), greatly simplifying experiments testing hundreds of different conditions and streamlining integration with robotic handling systems. Thus, compared to current single-cell RNA-sequencing technologies, PIP-seq has the greatest flexibility to cover combinations of cells and sample numbers (**Fig. 1g**).

Single-cell RNA-sequencing with particle-templated emulsification

To utilize PIPs for high-throughput single-cell sequencing requires efficient cell lysis and reverse transcription of mRNA using barcoded primers. In the absence of microfluidics, PIPs, cells, and

lysis reagents must be combined prior to emulsification. To prevent cell lysis before compartmentalization, we use Proteinase K (PK), a protease that has minimal activity at 4°C but that can be activated at higher temperatures. After emulsification, the sample is heated to efficiently lyse cells. To illustrate this process, we stained cells with calcein, encapsulated them at 4°C with Proteinase K using PIPs, and imaged the droplets before and after thermal activation. Intact cells appeared as compact puncta prior to lysis, but rapidly released calcein into the bulk of the droplets after the temperature was increased (**Fig. 2a**). Thus, cells can be mixed with PK in bulk prior to emulsification, and thermal activation triggers the release of mRNA for barcoding after emulsification.

To ensure that temperature-activated lysis and bulk agitation does not pre-lyse cells and result in mRNA cross contamination, we performed mouse-human cell line mixing studies. We synthesized barcoded polyacrylamide beads with polyT sequences, using split-pool ligation of four 6 bp randomers[30]. Beads contained ~10^8 (96^4) unique barcodes, providing ample sequence space to label a million cells. PIP-seq barcode rank plots for mixed mouse-human cell suspensions allowed cell identification by UMI abundance (**Fig. 2b**). The fraction of mouse reads in human transcriptomes was below 3%, and transcriptomes containing multiple cells were rare and consistent with Poisson encapsulation of two cells **(Fig. 2c-d)**. These results illustrate that PIP-seq yields high purity single-cell RNA-seq data with minimal transcriptome mixing and low doublet formation.

Accurate reconstruction of single-cell phenotypes in breast tissue

An important application of single-cell sequencing is atlasing cell types in a complex tissue. To investigate the feasibility of atlasing studies, we applied PIP-seq samples derived from healthy

breast tissue. In tandem, we performed scRNA-seq on tissues from the same patients using a commercially available scRNA-seq technology (10x Genomics, Chromium v3). We integrated PIP-seq data across participants and recovered expected cell types by dimensionality reduction, including the two lineages of luminal epithelial cells (LEP1 and LEP2), myoepithelial cells, fibroblasts, vascular cells, and immune cells **(Fig. 3a, Extended data Fig. 2a,b)**[31]. To compare transcriptome capture between platforms, we downsampled the 10x Chromium and PIP-seq datasets to an equivalent number of cells and reads (2400 cells, 7k reads per cell). Chromium detected more genes (1261 *vs*. 1134) and transcripts (2918 *vs*. 1938) per cell, with similar percentages of reads assigned to mitochondrial transcripts (2.85% *vs*. 1.19%) **(Extended data Fig. 2c)**. To compare the transcriptome accuracy of PIP-seq, we downsampled each dataset to an equivalent number of unique molecular identifiers (UMIs) per cell (2400 cells, 1500 UMIs), integrated the data, performed dimensionality reduction, and cluster identification. We compared marker genes and the correlation between gene expression profiles by cluster. Predicted marker genes were concordant between methods **(Fig. 3d)**, gene expression was highly correlated **(Fig. 3e, Extended data Fig. 3a)**, and breast tissue markers from previous reports segregated identically within integrated clusters **(Extended data Fig. 3b).** Thus, PIP-seq can accurately profile complex tissues.

PIP-seq for single-cell pooled CRISPR screens

CRISPR perturbations combined with single-cell sequencing allows unbiased discovery of genotype-phenotype relationships[32-34]. Expanding this approach to genome-wide sgRNA libraries can elucidate gene function on an unprecedented scale. However, such studies require sequencing millions of cells to characterize all perturbations in libraries with tens or hundreds of

thousands of individual sgRNA[19]. To demonstrate how the throughput of PIP-seq enables perturbation studies at scale, we profiled the transcriptional changes associated with a CRISPR interference allelic series CROP-seq library. This library expressed sgRNA and a polyadenylated copy of the guide sequence from separate promoters. Guide RNAs were captured and barcoded with the cell's polyadenylated mRNA, making this approach immediately compatible with PIP-seq. The library is designed to quantitatively titrate gene expression using sgRNAs with target site mismatches[35], allowing us to compare measured gene expression to expected knockdown efficiency across each gene's allelic series **(Fig. 4a).** We transduced K562 cells containing a stable dCas9-KRAB with the CRISPRi lentiviral library and performed PIP-seq to capture the transcriptional profiles and sgRNA identity of individual cells **(Fig. 4b-c)**. For cells with single gRNA assignments, previously reported knockdown efficiencies[35] correlated with the normalized counts of targeted genes **(Fig. 4d)** and were most significant for highly expressed genes **(Extended data Fig. 4a,b).** In addition, knockdown of genes produced known transcriptional changes. For example, gRNA targeting HSPA5 resulted in endoplasmic reticulum stress and increased unfolded protein response **(Fig. 4e).** These results validate use of PIP-seq for CROP-seq experiments, paving the way for routine million cell experiments that map genotype-phenotype relationships at genome-scale.

PIP-seq identifies unique single-cell transcriptomic signatures correlated with the relapse of mixed phenotype acute leukemia (MPAL)

Monitoring of cancer in response to therapy is an emerging application of single-cell sequencing that benefits from rapid sample processing at the point of collection, and the ability to delay cDNA synthesis and library preparation until multiple samples have been collected. We

investigated the utility of PIP-seq for understanding cancer dynamics by first validating the single-cell transcriptional responses of two cancer cell lines (H1975, PC9) to Gefitinib, an epidermal growth factor receptor (EGFR) tyrosine kinase inhibitor. We treated H1975 and PC9 with DMSO (vehicle control) or 1 μM Gefitinib overnight and performed PIP-seq **(Fig. 5a)**. A transcriptional response in H1975, which is resistant to Gefitinib due to EGFR mutations L858R and T790M, was not observed, while Gefitinib sensitive PC9 cells showed a substantial shift in gene expression **(Fig. 5b).** Differential gene expression analysis revealed increased levels of *TACSTD2* (*TROP2*) in PC9 cells, consistent with its known modulation during lung adenocarcinoma tumor growth[36] **(Fig 5c)**, and decreased expression of *CDK4*, which is known to enhance sensitivity to EGFR inhibitors[37] (**Extended data Fig. 5)**. In addition, drug resistant H1975 cells spiked into a background of sensitive cells (1:9 H1975:PC9) could be detected solely by their single-cell phenotypes, and at roughly the expected frequency (4.7%) **(Fig. 5d)**. Thus, PIP-seq recovered genes with reported roles in lung-cancer drug resistance and could identify resistance phenotypes within a background of drug-sensitive cells.

Next, we applied PIP-seq to study mixed phenotype acute leukemia (MPAL), a high-risk disease characterized by multiple hematopoietic lineages[38,39]. Recurrence and changes in immunophenotype with chemotherapy are typically monitored using flow cytometry of surface markers during diagnosis, treatment, and relapse, but this provides limited insight into the drivers of relapse after drug treatment. Like other single-cell RNA-seq methods, PIP-seq can be multiplexed to simultaneously characterize single-cell gene expression and surface immunophenotype[40]. Using PIP-seq, we performed antibody-derived tag (ADT) sequencing (CITE-seq) on longitudinal samples collected from MPAL patients treated with chemotherapy. PIP-seq confirmed the diagnosis of these samples as B/myeloid MPAL and identified aberrant

expression of immune and stem cell markers that matched with clinical immunophenotypes determined by flow cytometry **(Supplemental Table 2, Extended data Fig. 6)**. However, PIP-seq revealed an additional layer of complexity undetectable by traditional immunophenotyping. Dimensionality reduction identified new cell clusters that emerged after drug treatment **(Fig. 5e,f, Extended data Figs. 7, 8)**. These clusters had similar immunophenotypes **(Fig. 5g,h)**, but contained significant transcriptional heterogeneity **(Fig. 5i,k, Supplemental Tables 3,4)**. Cell populations up-regulating genes and pathways (oxidative phosphorylation, G2M checkpoint modulation, ribosome biogenesis) **(Fig. 5j,l)** implicated in a variety of cancers including acute lymphoblastic leukemia[41-50], but not previously linked to MPAL, were observed. Taken together, our results highlight the value of single-cell methodologies for studying the heterogeneous response of cancer subpopulations to chemotherapy, and the potential for integration of simple and reliable scRNA-seq workflows into clinical research.

Discussion

Genomics has progressed rapidly to high throughput, multi-modal, single-cell analysis[40,51-54]. Further improvements in data quality, the ability to measure additional cellular properties, and new computational approaches for understanding and integrating single-cell information[55-57] will continue to refine our understanding of cell states. At the same time, there remains an unmet need for simplified workflows that scale in cell number and sample size, and that allow for breaks in processing after initial sample collection. PIP-seq is a microfluidics-free, single-cell RNA-sequencing method that produces high-quality data using a drastically simplified emulsification technique. Like other high-throughput single-cell approaches, PIP-seq is fundamentally a strategy to barcode mRNA from cells so that material can be pooled and

sequenced. The core advantage of PIP-seq is the speed and simplicity of sample processing. Pre-templated instant partitions form monodispersed emulsions in minutes with a standard laboratory vortexer, removing the need for instrumentation located in core-facilities or hours of multichannel pipetting to perform split-pool indexing in plates. This expands access to single-cell technologies in several important ways. It reduces the need for sample transport, enabling immediate processing by technicians without prior training, and collection and banking of samples from remote locations, including field sites. It allows infectious samples that require special precautions to be processed at the point of collection or in the biosafety facilities where they are stored. More generally, rapid sample processing eliminates the need for fixatives and minimizes transcriptional perturbations and batch artifacts associated with processing many samples in series.

In addition to workflow simplicity, PIP-seq is intrinsically scalable, handling cell inputs over five orders of magnitude ($10\text{-}10^6$), making it well suited for screening, genome-wide Perturb-seq experiments, and large cell-atlasing studies. While methods based on combinatorial indexing scale efficiently to large cell numbers, PIP-seq has a substantially simpler workflow and is also compatible with high throughput processing of samples in plates, allowing many conditions and replicates to be run simultaneously. This has important implications for data quality and biological discovery in single-cell experiments since detection of true positives and reduction in false positives in differential expression analysis is substantially improved by incorporating replicates and statistical methods that account for biological variability[58]. Increased flexibility in the number of samples that can be processed also enables previously intractable experimental designs, like dose-response curves, time-course studies, combinatorial perturbations, single-cell sequencing of organoids, and large drug screens. In addition, because

PIP-seq can directly emulsify in plaes, it integrates with robotic fluid handling and therefore comprises a drop-in solution for single-cell readouts in high-throughput experiments in academia or industry.

We confirmed the accuracy of PIP-seq as a single-cell genomics tool by profiling heterogeneous tissue and directly comparing our results to the leading scRNA-seq platform (10x Genomics). PIP-seq cell type classification, marker identification, and gene expression levels were tightly matched with 10x data but detected fewer genes per cell. We attribute these differences to the extensive optimization that the commercial 10x platform has undergone and suspect that, like other single-cell techniques[3-6,12,25,59], further improvements to PIP-seq molecular biology will increase sensitivity. In addition, because PIP-seq emulsions are functionally equivalent to those made with microfluidics, the approach is immediately compatible with emerging advances, including improvements to the molecular biology of myriad multi-omic profiling methods developed for other droplet microfluidic barcoding systems[40,57,60].

Finally, we demonstrate the utility of PIP-seq in processing clinical samples. In combination with barcoded antibodies, we profiled the relapse of mixed phenotype acute leukemia (MPAL) after chemotherapy. MPAL is a subtype of leukemia characterized by poor prognosis[61], lineage ambiguity, lack of consensus regarding therapy, and significant intratumoral genetic and immunophenotypic heterogeneity[62]. The molecular mechanisms underlying treatment resistance in this complex disease remain undefined. Changes in gene expression have been linked to prognosis and treatment resistance in multiple cancers. However, tumor heterogeneity makes it unlikely that bulk sequencing methods would identify strong gene signatures associated with resistance in clinical samples. Using PIP-seq of samples from two individuals with MPAL with disease progression after initial therapy, we identified

transcriptional heterogeneity beyond that observed by immunophenotype and speculate that this heterogeneity may play a role in MPAL treatment resistance. We observed up-regulation of genes and pathways previously associated with acute lymphoblastic leukemia in several cell subsets that emerged after chemotherapy, as well modulation of ribosomal genes in both patients. Control of translation has been previously implicated in many cancers[41-46,63], including leukemia, but has not yet been linked to MPAL progression and drug resistance, suggesting that new therapeutics targeting ribosomal biogenesis and/or protein translation may also have therapeutic potential in MPAL[64]. Our results motivate the use of single-cell technologies for understanding MPAL tumor heterogeneity and response to chemotherapy and suggest that the broad adoption of such technologies for monitoring cancer progression (and tailoring treatment) is within reach. In summary, single-cell RNA-sequencing provides unparalleled insight into cell heterogeneity but remains underutilized in many settings. PIP-seq addresses this with a simple, rapid, and scalable workflow that can be used by any lab containing standard molecular biology equipment.

Methods

Proteinase K triggered cellular lysis and mRNA capture. Mammalian cells were stained with Calcein AM (ThermoFisher #C3099) in 1 mL of PBS with 0.04% BSA according to manufacturer's instructions. After 30 min of incubation at room temperature on a rotisserie incubator (Isotemp, Fisher Scientific), cell suspensions were quantified with a Luna-FL automated cell counter and diluted in 1X PBS with 0.04% BSA. 1500 calcein-stained cells in 5 µL of were added to 35 µL of PIPs with 29 U/mL Proteinase K (NEB #P8107S) and 70 mM DTT (Sigma #D9779) and mixed for 10 pipet strokes. Care was taken to avoid generating bubbles when mixing cells with PIPs. 280 µL of 0.5% ionic Krytox in HFE 7500 oil[65] was added

to the cell-bead mixture and vortexed at 3000 RPM for 15 seconds horizontally and then 2 minutes vertically a custom vortexer (Fluent BioSciences, #FB0002776). Oil was removed from below the emulsion such that less than 100 µL remained. The PIP emulsion was subsampled on a C-Chip disposable hemacytometer (Fisher Scientific # DHCN015) before lysis with each subsample consisting of 3.5 µL of PIP emulsion per field of view. The C-chip was imaged in bright-field at 2X magnification. The remaining PIP emulsion was subjected to enzymatic lysis at 65°C for 35 min on a PCR thermocycler (Eppendorf Mastercycler Pro) with lid temperature set to 105°C. After lysis was complete, fluorescence images were captured using a Nikon 2000 microscope with 470 nm excitation (Thorlab M470L5).

Varied format emulsification. PIP emulsification in varied formats was performed in 1.5 mL microcentrifuge tubes, 15 mL conical tubes and 50 mL conical tubes. Briefly, PIP particles were suspended in buffer with 29 U/mL Proteinase K Proteinase K (NEB #P8107S) and 70 mM DTT (Sigma #D9779) and pelleted through centrifugation. PIPs were then distributed at 200 uL, 2 mL and 8 mL volumes in 1.5 mL, 15 mL and 50 mL tubes, respectively. Fluorinated oil with surfactant (Fluent Biosciences # FB0001804) was added to each tube at 1 mL, 8 mL and 32 mL volumes, respectively. Emulsification was conducted on a Vortex Genie 2 with a custom adapter at 3000 rpm for 1 min. After emulsification, the samples were allowed to settle for 30 seconds, and excess oil was removed via syringes using G22 blunt needles. The emulsion was subsampled, loaded on a C-Chip disposable hemacytometer (Fisher Scientific #DHCN015), and imaged under brightfield microscopy (DIAPHOT300, Nikon) at 2x and 4x magnification.

PIP emulsification in well plates was performed in 96, 384, and 1536 well plates. Briefly, PIP particles were suspended in 2% (v/v) Triton X-100 (Sigma, X100-5ML) in 10 mM TrisHCl

(Teknova, T1075), then centrifuged at 6000 rcf, and supernatant removed. Depending on the well plate working volume, 38 µL, 8 µL, or 3 µL of the centrifuged PIPs was added to 96, 384, or 1532 well plates respectively. For 96 and 384 well plates 2 µL of sample was added to each well, for 1532 well plates, 1 µL was added to each well. PIP and sample volumes totaled 25% of the volume of each well. The plate was then sealed (Applied Biosystems, 4306311) and shaken for 5 min (IKA, 253614 and 3426400) to ensure complete mixing. Well plates were centrifuged at 200 rcf for 1 min before removing the seal. Then 80 µL, 20 µL, or 8 µL 2% (w/w) fluorosurfactant (Ran BioTechnologies, 008 Fluorosurfacant) in HFE oil (3M, Novec 7500) was added to each well in 96 (Applied Biosystems, N8010560), 384 (Applied Biosystems, A36931), or 1532 (Nunc, 253614) well plates respectively. The addition of oil represented 50% of the volume of each well for a total volume of 75% consisting of PIP, sample, and oil. After resealing, PIP emulsification was performed by vortexing for 30 seconds at 3200 rpm (Benchmark Scientific, BV1003). The emulsified plate was centrifuged at 200 rcf for 1 min before removing the seal and imaging droplets from individual wells on a fluorescence microscope (EVOS FL Auto).

PIP-seq. Pre-aliquoted barcoded PIPs were thawed on ice. Unless otherwise noted, cells were centrifuged 300 x g for 5 min, washed twice in 1X PBS without calcium or magnesium (ThermoFisher #70011044) with 0.04% BSA, filtered with a 70µmcell strainer, and resuspended in 1X PBS with 1% Pluronic F127 (Sigma #P2443). *For the human:mouse mixing study*, human HEK 293T cells (ATCC # CRL-3216) were grown in DMEM (ThermoFisher #11995073) supplemented with 10% FBS (ThermoFisher #A3840001) and 1% Penicillin-Streptomycin-Glutamine (ThermoFisher #10378016). Murine NIH/3T3 cells (ATCC # CRL-1658) were grown

in DMEM (ThermoFisher #11995073) supplemented with 10% bovine calf serum (ATCC # 30-2030) and 1% Penicillin-Streptomycin-Glutamine. Cells were grown to a confluence of ~70% and treated with TrypLE Express with Phenol red (ThermoFisher #12605010) for 3 minutes, quenched with an equal volume of growth medium, and centrifuged at 5 min at 200 x g. The supernatant was removed, and the cells resuspended in 1X DPBS without calcium or magnesium. Cells were diluted to their final concentration in 1X DPBS with 0.04% BSA and mixed evenly to create a 50:50 Human:Mouse mixture. Cell viability was evaluated using acridine orange/propodium iodide stain (Logos Bio # F23001) and quantified with a Luna-FL automated cell counter. *For the lung adenocarcinoma study*, 5 µL of cells (400 cells/µL) were added to 28 µL of PIPs with 22.8 U/mL Proteinase K and 28 mM DTT and mixed for 10 pipet strokes. 150 µL of 0.5% ionic Krytox in HFE 7500 oil[65] was added to the cell-bead mixture and it was vortexed at 3000 RPM for 1 minute on a Vortex Genie 2 with a custom tube adapter. Care was taken to avoid generating bubbles when mixing cells with PIPs. For the CROP-seq study, 3 µL of cells (333 cells/µL) was added to 28 µL of PIPs with 29 U/mL Proteinase K and 70 mM DTT and mixed for 10 strokes. 150 µL of 0.5% ionic Krytox in HFE 7500 oil was added to the cell-bead mixture and it was vortexed at 3000 RPM for 1 minute on a Vortex Genie 2 with a custom tube adapter. *For the healthy breast tissue study*, 20 µL of cells (625 cells/µL) was added to 200 µL of PIPs and mixed for 10 strokes. *For the 72 hour hold experiment*, 5 µL of a 50:50 mixture of human HEK 293T cells and murine NIH/3T3 cells (500 cells/µL) was added to 35 µL of PIPs with 29 U/mL Proteinase K and 70 mM DTT and mixed for 10 strokes. 280 µL of oil (Fluent Biosciences # FB0001804) was added to the cell-bead mixture and it was vortexed on a digital vortexer using a custom adapter at 3000 rpm for 15 seconds horizontally and 2 minutes vertically. 230 µL of excess oil was removed and the emulsion was placed on a pre-heated digital

dry bath at 65°C for 35 min and 4°C for 30 minutes. Control samples proceeded to emulsion breaking while 0°C hold samples were placed in an ice bucket in the 4°C refrigerator for 72 hours prior to breaking emulsions.

Unless otherwise note, for all formats, oil was removed from below the emulsion such that less than 100 µL remained and enzymatic lysis was completed at 65°C for 35 minutes with a 4°C hold on a PCR thermocycler with lid temperature set to 105°C. The remaining oil was removed. The emulsion was broken as follows. Using a multichannel pipet, 180 µL of high salt buffer (250 mM Tris-HCl pH 8, 375 mM KCl, 15 mM MgCl2, 50 mM DTT) at room temperature was added to the top of the emulsion followed by 40 µL of 100% 1H,1H,2H,2H-perfluoro-1-octanol (Sigma Aldrich, 370533). The samples were vortexed for 3 seconds, briefly centrifuged on a benchtop plate spinner, and the bottom oil phase was removed. PIPs were transferred into a 1.5 ml Eppendorf tube and washed 3 times with 2x RT buffer (100 mM Tris-HCL pH 8.3, 150 mM KCl, 6 mM MgCl2, 20 mM DTT) with 1% Pluronic F68 (Gibco #24040032). After washing, the beads were pelleted, aqueous removed, and the remaining bead and buffer volume was 25 ul. To this mix, 25 µL of Reverse transcription Master Mix (4.8% PEG8000, 4% PM400, 2.5 µM template switch oligo (PIPS_TSO), 1 mM dNTPs, 1 U/µL RNase Inhibitor, 1 U/µL reverse transcriptase enzyme) was added, mixed, and cDNA synthesis was completed for 30 minutes at 25°C, 90 minutes at 42°C, followed by 10 minutes at 85°C and a 4°C hold. Whole transcriptome amplification (WTA) was performed directly on RT product without purification by adding 50 µL of 1x KAPA Hifi master mix, 0.25µMprimer (PIPS_WTA_primer) and thermocycling 95°C for 3 min, then 16 cycles of (98°C 15 s, 67°C 20s, 68°C 4 min) followed by 72°C 5 min and 4°C hold. After WTA, PIPs were filtered using Corning Spin-X filter columns (1 min at 13,000 xg) and purified using 0.6x Ampure XP.

Libraries were generated from WTA amplified material using the Nextera XT DNA Library Preparation Kit with a custom primer (PIPs_P5library) and standard Nextera P7 indexing primers (N70x). Libraries were pooled and sequenced using an Illumina NextSeq 2000 instrument with 15% PhiX. Oligonucleotides used in this study are found in **Supplemental Table 1**.

Analysis of healthy breast tissue. Fresh reduction mammoplasty tissue was processed as previously described[31,66]. Bulk mammary tissues were mechanically processed into a slurry and digested overnight with collagenase type 3 (200U/mL, Worthington Biochem CLS-3) and hyaluronidase (100U/mL, Sigma-Aldrich H3506) in medium containing charcoal:dextran stripped FBS (GeminiBio 100-119). The digested fragments were size filtered into sub-40 micron fraction and above 100 micron fraction and cryopreserved. For PIP-seq, cells were thawed and then resuspended in PBS + 0.04% BSA and passed through a 70 micron FlowMi cell strainer (Sigma # BAH136800070). Then cells were counted and diluted with PBS + 0.04% BSA to a concentration of 1500 cells/µL. For each sample, 20 µL of cell suspension (625 cells/µL) was input into 200 µL of PIPs. mRNA extraction and reverse transcription was performed under the same conditions as previously described. Whole-transcriptome amplification was performed with the following thermocycler protocol: 95°C 3m, 16 cycles of [98°C 15s, 69°C 4m 20s], 72°C 5m. Following cDNA isolation as previously described, 50 ng of cDNA was used as input into library preparation. Samples were sequenced on the Illumina NextSeq 2000, with four patient samples pooled per P3 cartridge and sequenced at a read depth of approximately 7,000 reads/cell. For 10x Genomics data, the 100-micron fraction were thawed, then further digested with trypsin, followed by dispase (Stemcell Technologies #07913) and DNAseI (Stemcell Technologies #07469) digestion to achieve single-cell suspension. Cells from each patient were labeled with MULTIseq barcodes[13], then pooled and stained with DAPI to be sorted for DAPI- live cells. Single-cell libraries were prepared according to the 10X Genomics Single Cell V3 protocol (v3.1 Rev D) with the standard MULTIseq sample multiplexing protocol. The libraries were sequenced on a NovaSeq S4 lane at a read depth of about 70,000 reads/cell. To compare

platforms, we downsampled PIP-seq and 10x data, which had different numbers of cells and sequencing depth per cell. The PIP-seq data had 54,825 cells, sequenced at approximately 7k reads per cell, while the 10x data had 2420 cells sequenced at approximately 70k reads per cell. Data were downsampled to 2400 cells and 7k reads in R (downsampleReads, DropletUtils) to compare the number of genes and transcripts detected. Data were downsampled to 2400 cells and 1500 UMIs in R (SampleUMI, Seurat v4.1.0) to compare the accuracy of marker gene detection.

CROP-seq. K562 CRISPRi cells were cultured in RPMI-1640 (Gibco #11875093) with 10% FBS (Thermo Fisher Scientific, #10438026) and 1% penicillin/streptomycin (Thermo Fisher Scientific, #15140148) in an incubator at 37°C with 5% CO2. K562 CRISPRi cells were transduced with a lentivirus library containing 138 sgRNA[35] at a multiplicity of infection of 0.1. Lentivirus infected cells (BFP+) were sorted to high purity using a BD FACS Aria III (100 µMnozzle) and processed according to the PIP-seq scRNA-seq workflow. cDNA was processed according to the standard protocol to obtain sequence ready libraries containing transcriptome information. To recover sgRNA sequences, we implemented an additional amplification step. We amplified 1 ng cDNA in a 50 µL reaction using of primers P5-PE1 (0.5uM) and Weissman_U6 (0.25uM) **(Supplementary Table 1)** with 1x Kappa HIFI. Reactions were thermocycled at 95°C for 3 min followed by 10 cycles of [95°C for 20s, 70°C for 30s [-0.2°C per cycle], 72°C for 20s], followed by 8 cycles of [95°C for 20s, 68°C for 30s, 72°C for 20s], followed by 72°C for 4 minutes, and 4°C forever. Library PCR product enriched in sgRNA sequences was purified with a double sided 0.5x/0.8x Ampure XP bead cleanup and the size was determined (Agilent Tapestation).

Transcriptome and sgRNA libraries were pooled at 20:1 before sequencing. Reads were first processed to extract sgRNA sequences. The bioinformatics pipeline was run using a custom index built from the full human transcriptome (GENCODE v32) and guide RNA sequences (salmon v1.1.0.) (**Supplemental Table 1**). This approach led to the recovery of >14,000 unique gRNA counts across all cell-associated barcodes. Cells were assigned to gRNA groups using a previously reported approach [32]. Briefly, cells were classified as uniquely expressing a single gRNA species if the guide's expression was at least 10-fold higher than the sum of all other gRNAs. Similarly, cells were classified as containing multiple gRNAs in cases where the difference was smaller than one. For the 581 single cells sequenced, 2 did not have any gRNA, 441 contained a single gRNA, and 138 contained multiple gRNA. Cell barcodes were processed using Seurat v4.1.0. All gRNAs in the list of features were excluded from identification of variable transcripts (feature selection) and in subsequent stages of dimensionality reduction and clustering. To understand the relationship between gRNAs and mRNA expression, gRNAs were ranked according to their expected level of knockdown, reported previously[35], and a generalized additive model was used to assess groupwise trends for each set of gRNAs.

Lung adenocarcinoma cell line experiments. PC9 was obtained from the RIKEN Bio Resource Center (#RCB4455). H1975 was obtained from the American Type Culture Collection (#CRL-5908). Cells were cultured in RPMI-1640 (Gibco #11875093) with 10% fetal bovine serum (FBS), penicillin, and streptomycin in an incubator at 37°C with 5% CO2. 1 µMGefitinib (Frontier Scientific, 501411677) or DMSO was added to culture flasks 24 hours before cells were harvested for processing. PC9 and H1975 were both treated with Gefitinib and DMSO. To perform the cell mixing study, Gefitinib treated H1975 and Gefitinib treated PC9 were mixed at

a ratio of 1:9 H1975:PC9. Cells were processed according to the PIP-seq scRNA-seq workflow described above. Triplicate tubes of 400 cells were processed per treatment condition. Data was analyzed using Seurat v4.1.0.

Mixed phenotype acute leukemia (MPAL). Patients whose samples were used in this study were treated at the University of California San Francisco. Samples were collected in accordance with the Declaration of Helsinki under institutional review board-approved tissue banking protocols, and written informed consent was obtained from all patients. Cryopreserved peripheral blood mononuclear cells and peripheral bone marrow mononuclear cell samples were thawed by hand until approximately 85% of ice remained. Using a 5 mL serological pipette, 1 mL of 4°C defrosting media (DMEM with 20% FBS and 2 mM EDTA) was added dropwise to each sample and then, without disturbing the remaining ice pellet, the sample was carefully transferred dropwise to a pre-prepared 40 mL aliquot of 4°C defrosting media. This was repeated until the contents of the entire cryovial were transferred into the 50 mL conical of defrosting media. The sample was inverted 4-5 times and centrifuged at 114 x g for 15 min at 4°C with no brake. The supernatant was aspirated and 10 mL of room temperature RPMI 1640 with 1% Penicillin-Streptomycin-Glutamine was used to gently resuspend the cells. Cell clumps were manually removed, and if necessary cells were filtered through a 70 micron cell strainer into a fresh 50 mL conical. The sample was inverted 2-3 times and centrifuged at 114 x g for 10 minutes with low brake at room temperature. The supernatant was aspirated and cells were resuspended in an appropriate volume of 1X PBS + 5% FBS. Cells were quantified with AO/PI and viability evaluated on the Luna-FL. 1-2 million cells were aliquoted into a new 15mL conical and then centrifuged at 350 x g for 4 min at 4°C and then the supernatant was aspirated

and the tube was placed on ice. 45 µL of cold Cell Staining Buffer (BioLegend, 420201) was added per million cells and resuspended gently. 5 µL Trustain FcX block (BioLegend, 422301) was added per million cells and gently mixed 10 times with a wide-bore pipette tip. Cells were blocked on ice for 15 minutes. A custom pool of 19 TotalSeq A antibodies was obtained from BioLegend. Immediately prior to use, antibodies were mixed and centrifuged at 10,000 x g for 4 min at 4°C. 4.6 µL of 0.5 µg/µL antibody pool was added per million of the blocked cells and gently mixed 10 times with a wide-bore pipette tip. The samples were incubated on ice for 60 minutes. Next, 3.5 mL of cold Cell Staining Buffer was added, gently mixed with a wide-bore pipette tip, and slowly inverted twice to mix. Cells were centrifuged at 350 x g for 4 min at 4°C and then the supernatant was removed. Addition of cold Cell Staining buffer was repeated twice for a total of 3 washes. After the final supernatant aspiration, stained cells were resuspended in 1X PBS with 0.04% BSA and mixed 5-10 times until cells were completely suspended without visible clumps. Cell concentration was determined with AO/PI and viability evaluated on the Luna-FL. Final dilutions were made in 1X PBS with 0.04% BSA. 20 µL of cells was added to 200 µL of PIPs (1000 cells/µL) and processed using the standard PIP-seq workflow described above.

PIP-seq bioinformatic analysis. Analysis of sequencing data was performed using custom scripts to generate gene expression matrices starting from processed fastq sequences. The pipeline comprises 4 basic steps: barcode identification and error correction, mapping to reference sequences, cell calling, and gene expression matrix generation. Briefly, after demultiplexing the sequencing data each read in the fastq is matched against a “whitelist” of known barcodes. Reads were matched with a hamming distance tolerance of 1, meaning that the

barcode portion of a read can differ from a whitelist entry by one base and still be matched to that barcode. Reads that do not match any barcode in the whitelist were discarded from further analysis. Matching reads were output to a new, intermediate fastq file that was then used for mapping against an appropriate transcriptome reference. Reference transcriptomes matching the species of each sample were prepared using the Salmon *index* function with the default k-mer size of 31[67]. Gencode references were used to build the transcriptome indexes including GRCh38.p13 for human, GRCm38.p6 for mouse, and the combination thereof for HEK/3T3 cell mixture studies. Following barcoding, Salmon *alevin* v1.2.0[68] was used to map reads to the full transcriptome. The intermediate fastq generated during barcoding were provided as input into *alevin* along with a list of all whitelisted barcodes contained in raw reads. After mapping, data were output as a UMI counts matrices (sparse matrix, gene list, barcode list) with size *all barcodes x all genes in index*. An in-house python implementation of emptyDrops[69], a standard scRNA-seq method to separate putative cells from background, was then applied. A custom threshold for each experiment was set, beneath which no true cell calls are expected to fall. As with emptyDrops, an estimated ambient profile across all barcodes beneath that threshold was created. A p-value was computed by comparing the gene expression profile for each barcode above the threshold against the ambient profile. Barcodes that have a statistically significant difference (Benjamini-Hochberg adjusted-$p<0.001$) from the ambient background profile are categorized as cell-containing barcodes. The *alevin* output matrices are then subset to only include called cell barcodes. The Seurat package (v4.1.0) was used to perform downstream clustering, marker gene determination, and visualization in R.

Figure 1. Rapid and scalable pre-templated emulsification for single-cell genomics. (a-d) PIP-seq enables the encapsulation, lysis, and barcoding of single cells. **(a)** Schematic of the emulsification process. Particle templates, cells, and lysis reagents are combined with oil and vortexed to generate monodispersed droplets. **(b)** Heat activation of Proteinase K results in lysis and release of mRNA that is captured on template-bound barcoded polyT oligonucleotides. **(c)** Oil removal is followed by bulk reverse transcription of mRNA into cDNA. **(d)** Barcoded whole transcriptome amplified cDNA is prepared for Illumina sequencing. **(e-g)** Efficient single bead, single drop encapsulation at scale. **(e)** PIPs encapsulation in different (1.5 ml, 15 ml, 50 ml) sized tubes produces monodispersed emulsions capable of barcoding orders of magnitude different cell numbers. **(f)** PIP-seq is compatible with plate-based emulsification, including 96-, 384- and 1536-well plate formats. **(g)** Estimated ability of different technologies to easily scale with respect to cell and sample number.

Figure 2. Heat-activated enzymatic lysis yields high purity single-cell transcriptomes. (a) Fluorescence microscopy (Brightfield, GFP) of calcein-stained cells emulsified with PIPs before and after heat-activated lysis. Inset: images show cell puncta (left) and release of calcein (right). **(b-d)** Cell purity assessed with mouse:human mixing studies. **(b)** The distribution of total UMIs as a function of cell barcode rank. **(c-d)** Purity analysis of cell transcriptomes assessed using barnyard plots with cells colored by cell type. Red points are mouse reads, blue points are human reads, and green points are mixed reads.

Figure 3. Accurate single-cell transcriptional profiling of healthy breast tissue using PIP-seq. (a) Clustering and identification of cell types from PIP-seq data (54,825 cells from 2 patients). **(b-e)** Comparison of PIP-seq to 10x genomics data collected from the same tissue. **(b)** Integration of PIP-seq and 10x data. **(c-d)** Cell clustering and comparison of marker genes between platforms. **(d)** Heatmaps of marker gene expression show similar patterns in PIP-seq and 10x data. **(e)** Correlations in normalized gene expression, by cluster, between platforms (see also Extended data Fig. 3).

Figure 4. Transcriptome and guide RNA sequencing using PIP-seq. (a) Schematic of the CROP-seq sgRNA library designed with target mismatches to modulate the activity of essential genes. **(b)** Lentiviral transduction of the CRISPRi library in K562 cells. **(c)** Schematic of the capture and barcoding of polyadenylated mRNA and sgRNA using PIP-seq. RNA and sgRNA libraries are prepared separately and pooled for sequencing. **(d)** Quantification of gene expression of sgRNA within an allelic series. sgRNA is ordered from high to low predicted knockdown efficiency (Jost et. al, 2020). Non-targeting sgRNA are denoted as "Null." **(e)** Preranked gene set enrichment analysis (GSEA) of scRNA-seq data comparing sgHSPA5 transduced cells to non-sgHSPA5 transduced cells shows enrichment in genes related to endoplasmic reticulum stress and unfolded protein response.

Figure 5. Molecular signatures of drug resistant cancer phenotypes in cell lines and patient samples. **(a)** A two-by-two experimental study design using lung adenocarcinoma cell lines (H1975, PC9) treated with Gefitinib or DMSO. **(b)** Clustering of single-cell RNA-seq after drug treatment shows transcriptional perturbations in Gefitinib-sensitive PC9, but not Gefitinib-resistant H1975 cells. **(c)** Increased expression of *TACSTD2* in PC9 challenged with Gefitinib. **(d)** Identification of drug-resistant H1975 cells spiked into drug-sensitive PC9 cells based on Gefitinib-induced transcriptional perturbation. **(e-l)** PIP-seq RNA and barcoded antibody (CITE-seq) analysis of mixed phenotype acute leukemia (MPAL). **(e)** Clustering of single cells for patient 65 before (left panel) and after (right panel) chemotherapy. (**f)** Clustering of single cells for patient 873 before (left panel) and after (right panel) chemotherapy. **(g-h)** Antibody derived tag (ADT) abundance, by cluster, before (t1) and after (t2) chemotherapy. ADTs change as a function of chemotherapy but are consistent among clusters for both patients, with the exception of T cell subsets. **(i-l)** Analysis of transcriptional heterogeneity in MPAL samples **(i)** Heatmap of top differentially expressed marker genes by cluster after relapse in patient 63. **(j)** GSEA pre-ranked analysis comparing transcriptomic differences between clusters 1 and 7 in patient 65 using gene sets HP Acute Leukemia (M35856), Hallmark G2M Checkpoint (M5901), Hallmark Oxidative Phosphorylation (M5936), amd GOCC Ribosome (M17089) **(k)** Heatmap of top differentially expressed marker genes by cluster after relapse in patient 873. **(l)** GSEA pre-ranked analysis comparing transcriptomic differences between clusters 3 and 5 in patient 873 using gene sets HP Acute Myeloid Leukemia (M36586)**,** GOCC Ribosome (M17089)**,** GOBP Oxidative Phosphorylation (M17089), and Abnormal Myeloid Leukocyte Morphology (M37711).

Extended data Figure 1. Flexible sample processing with PIP-seq. (a) Storage of droplets after emulsification for 72 hours at 0°C did not change quality metrics. **(b)** Microscope images of droplets from wells of a 384-well plate emulsification experiment.

Extended data Figure 2. Quality control analysis of PIP-seq using healthy breast tissue (a) Integration and clustering of 54,825 cells from 2 patients with 2 replicates per patient. **(b)** Number of unique genes, transcripts, percent mitochondrial reads, and percent ribosomal reads as a function of cluster. **(c)** Comparison between 10x and PIP-seq data after downsampling 2400 cells to 7k reads per cell.

Extended data Figure 3. Comparison, after down-sampling (2400 cells 1500 UMIs) of the larger breast tissue PIP-seq dataset to 10x Genomics data generated from identical samples. **(a)** Correlations in normalized gene expression, by cluster, between platforms. **(b)** Expression of marker genes overlayed on clusters is consistent between platforms.

Extended data Figure 4. (a) Gene expression for each sgRNA within an allelic series for all genes in the CRISPRi library. Each sgRNA is ordered from predicted high to low knockdown efficiency. Non-targeting sgRNA are denoted as "Null." **(b)** The relationship between gene expression and predicted knockdown of each gene. Expected changes in transcription across the allelic series were prominent in highly expressed genes. p-value represents the significance of the generalized additive model relating gRNA identity to knockdown efficiency for each gene.

Extended data Figure 5. Identification of Gefitinib-specific transcriptional responses in cancer cell lines. (a) Violin plots of median expression values for selected differentially expressed genes. **(b)** The expression of selected differentially expressed genes superimposed on H1975 and PC9 cell clusters.

Extended data Figure 6. Clinical flow cytometry and corresponding antibody derived tag (ADT) data for patients 65 and 873 with mixed phenotypical acute leukemia (MPAL).

Extended data Figure 7. Analysis of PIP-seq data from MPAL Patient #65. (a) Integration of replicates and time points. **(b)** Correlation between the number of cells in each cluster before and after relapse identifies expansion of clusters 1,4, and7. **(c)** Volcano plots showing differential gene expression, by cluster, between t1 (before treatment) and t2 (after relapse).

Extended data Figure 8. Analysis of PIP-seq data from MPAL Patient #873. (a) Integration of replicates and time points. **(b)** Correlation between the number of cells in each cluster before and after treatment identifies expansion of clusters 3 and 5. **(c)** Volcano plots showing differential gene expression, by cluster, between t1 (before treatment) and t2 (after relapse).

Tables

Supplementary Table 1. Oligonucleotides used in this study.

Supplementary Table 2. Clinical characteristics of study participants.

Supplementary Table 3. Marker genes for patient 65 clusters identified using combined t1 and t2 timepoints (FindAllMarkers Seurat v4.1.0, only.pos=TRUE, min.pct = 0.25, logfc.threshold = 0, test.use='bimod').

Supplementary Table 4. Marker genes for patient 873 clusters identified using combined t1 and t2 timepoints (FindAllMarkers Seurat v4.1.0, only.pos=TRUE, min.pct = 0.25, logfc.threshold = 0, test.use='bimod').

Acknowledgments: We thank members of the Abate laboratory for helpful advice and discussions. **Funding:** ICC was supported by K22AI152644 and DP2AI154435 from the NIH. This work was supported by grants 1R44GM145185, 1R43CA239978-01 and 1R43GM137648-01A1 to Fluent BioSciences. MJ was supported by K99GM130964 from the NIH. JMR was supported by F31NS115380 from the NIH. JSW was supported by NIH 1RM1 HG009490-01 and Howard Hughes Medical Institute.

Author contributions: Conceptualization, ICC, ARA; Methodology, ICC, KMF, RM, CD, ARA; Investigation, ICC, KMF, YX, DW, KTP, CDA, AO, JQZ, PH, VK, CP; Formal Analysis, ICC, CH, AM-Z; Resources KMF, RM, JMR, JSW, CCS, ZJG, ARA; Manuscript preparation, ICC, CCS, CACP, ARA; Supervision, ICC, KMF, RM, CCS, ZJG, ARA.

Competing interests: ARA filed a patent related to PIPs and is a founder of Fluent Biosciences. ICC consults for Fluent Biosciences and is on their Scientific Advisory Board. KMF, RM, YX, CH, AO, PH, JQZ, AM-Z, and CDA are employees at Fluent Biosciences and are working to commercialize the PIP-seq technology. MJ consults for Maze Therapeutics and Gate Biosciences. JMR consults for Maze Therapeutics and Waypoint Bio. JSW declares outside interest in 5 AM Venture, Amgen, Chroma Medicine, DEM Biosciences, KSQ Therapeutics, Maze Therapeutics, Tenaya Therapeutics, Tessera Therapeutics and Velia Therapeutics.

Data and materials availability: Sequencing data were deposited into GEO SuperSeries accession number GSE202919 and will be available after peer review. All code will be made available from the corresponding author on reasonable request.

References

1 Eberwine, J. *et al.* Analysis of gene expression in single live neurons. *Proc Natl Acad Sci U S A* **89**, 3010-3014, doi:10.1073/pnas.89.7.3010 (1992).

2 Tang, F. *et al.* mRNA-Seq whole-transcriptome analysis of a single cell. *Nature Methods* **6**, 377-382, doi:10.1038/nmeth.1315 (2009).

3 Hagemann-Jensen, M. *et al.* Single-cell RNA counting at allele and isoform resolution using Smart-seq3. *Nat Biotechnol* **38**, 708-714, doi:10.1038/s41587-020-0497-0 (2020).

4 Hahaut, V., Pavlinic, D., Cowan, C. & Picelli, S. Lightning Fast and Highly Sensitive Full-Length Single-cell sequencing using FLASH-Seq. *bioRxiv*, 2021.2007.2014.452217, doi:10.1101/2021.07.14.452217 (2021).

5 Picelli, S. *et al.* Full-length RNA-seq from single cells using Smart-seq2. *Nature Protocols* **9**, 171-181, doi:10.1038/nprot.2014.006 (2014).

6 Picelli, S. *et al.* Smart-seq2 for sensitive full-length transcriptome profiling in single cells. *Nature Methods* **10**, 1096-1098, doi:10.1038/nmeth.2639 (2013).

7 Ziegenhain, C. *et al.* Comparative Analysis of Single-Cell RNA Sequencing Methods. *Mol Cell* **65**, 631-643 e634, doi:10.1016/j.molcel.2017.01.023 (2017).

8 Macosko, E. Z. *et al.* Highly Parallel Genome-wide Expression Profiling of Individual Cells Using Nanoliter Droplets. *Cell* **161**, 1202-1214, doi:10.1016/j.cell.2015.05.002 (2015).

9 Zilionis, R. *et al.* Single-cell barcoding and sequencing using droplet microfluidics. *Nature Methods* **12**, 44-73, doi:10.1038/nprot.2016.154 (2016).

10 Rosenberg, A. B. *et al.* Single-cell profiling of the developing mouse brain and spinal cord with split-pool barcoding. *Science* **360**, 176-182, doi:10.1126/science.aam8999 (2018).

11 Cao, J. *et al.* Comprehensive single-cell transcriptional profiling of a multicellular organism. *Science* **357**, 661-667, doi:10.1126/science.aam8940 (2017).

12 Gierahn, T. M. *et al.* Seq-Well: portable, low-cost RNA sequencing of single cells at high throughput. *Nat Methods* **14**, 395-398, doi:10.1038/nmeth.4179 (2017).

13 McGinnis, C. S. *et al.* MULTI-seq: sample multiplexing for single-cell RNA sequencing using lipid-tagged indices. *Nat Methods* **16**, 619-626, doi:10.1038/s41592-019-0433-8 (2019).

14 Stoeckius, M. *et al.* Cell Hashing with barcoded antibodies enables multiplexing and doublet detection for single cell genomics. *Genome Biol* **19**, 224, doi:10.1186/s13059-018-1603-1 (2018).

15 Consortium, T. T. S. & Quake, S. R. The Tabula Sapiens: a multiple organ single cell transcriptomic atlas of humans. *bioRxiv*, 2021.2007.2019.452956, doi:10.1101/2021.07.19.452956 (2022).

16 Haniffa, M. *et al.* A roadmap for the Human Developmental Cell Atlas. *Nature* **597**, 196-205, doi:10.1038/s41586-021-03620-1 (2021).

17 Melms, J. C. *et al.* A molecular single-cell lung atlas of lethal COVID-19. *Nature* **595**, 114-119, doi:10.1038/s41586-021-03569-1 (2021).

18 Han, X. *et al.* Construction of a human cell landscape at single-cell level. *Nature* **581**, 303-309, doi:10.1038/s41586-020-2157-4 (2020).

19 Replogle, J. M. *et al.* Mapping information-rich genotype-phenotype landscapes with genome-scale Perturb-seq. *bioRxiv*, 2021.2012.2016.473013, doi:10.1101/2021.12.16.473013 (2021).

20 Heath, J. R., Ribas, A. & Mischel, P. S. Single-cell analysis tools for drug discovery and development. *Nat Rev Drug Discov* **15**, 204-216, doi:10.1038/nrd.2015.16 (2016).

21 Cao, J. *et al.* The single-cell transcriptional landscape of mammalian organogenesis. *Nature* **566**, 496-502, doi:10.1038/s41586-019-0969-x (2019).

22 Utada, A. S., Fernandez-Nieves, A., Stone, H. A. & Weitz, D. A. Dripping to jetting transitions in coflowing liquid streams. *Physical review letters* **99**, 094502, doi:10.1103/PhysRevLett.99.094502 (2007).

23 Clark, I. C. & Abate, A. R. Microfluidic bead encapsulation above 20 kHz with triggered drop formation. *Lab Chip* **18**, 3598-3605, doi:10.1039/c8lc00514a (2018).

24 Datlinger, P. *et al.* Ultra-high-throughput single-cell RNA sequencing and perturbation screening with combinatorial fluidic indexing. *Nat Methods* **18**, 635-642, doi:10.1038/s41592-021-01153-z (2021).

25 Aicher, T. P. *et al.* Seq-Well: A Sample-Efficient, Portable Picowell Platform for Massively Parallel Single-Cell RNA Sequencing. *Methods Mol Biol* **1979**, 111-132, doi:10.1007/978-1-4939-9240-9_8 (2019).

26 Amini, S. *et al.* Haplotype-resolved whole-genome sequencing by contiguity-preserving transposition and combinatorial indexing. *Nature Genetics* **46**, 1343-1349, doi:10.1038/ng.3119 (2014).

27 Cusanovich, D. A. *et al.* Multiplex single cell profiling of chromatin accessibility by combinatorial cellular indexing. *Science* **348**, 910-914, doi:10.1126/science.aab1601 (2015).

28 Ding, J. *et al.* Systematic comparison of single-cell and single-nucleus RNA-sequencing methods. *Nat Biotechnol* **38**, 737-746, doi:10.1038/s41587-020-0465-8 (2020).

29 Hatori, M. N., Kim, S. C. & Abate, A. R. Particle-Templated Emulsification for Microfluidics-Free Digital Biology. *Anal Chem* **90**, 9813-9820, doi:10.1021/acs.analchem.8b01759 (2018).

30 Delley, C. L. & Abate, A. R. Modular barcode beads for microfluidic single cell genomics. *Sci Rep* **11**, 10857, doi:10.1038/s41598-021-90255-x (2021).

31 Murrow, L. M. *et al.* Changes in epithelial proportions and transcriptional state underlie major premenopausal breast cancer risks. *bioRxiv*, 430611, doi:10.1101/430611 (2020).

32 Datlinger, P. *et al.* Pooled CRISPR screening with single-cell transcriptome readout. *Nat Methods* **14**, 297-301, doi:10.1038/nmeth.4177 (2017).

33 Dixit, A. *et al.* Perturb-Seq: Dissecting Molecular Circuits with Scalable Single-Cell RNA Profiling of Pooled Genetic Screens. *Cell* **167**, 1853-1866 e1817, doi:10.1016/j.cell.2016.11.038 (2016).

34 Replogle, J. M. *et al.* Combinatorial single-cell CRISPR screens by direct guide RNA capture and targeted sequencing. *Nat Biotechnol* **38**, 954-961, doi:10.1038/s41587-020-0470-y (2020).

35 Jost, M. *et al.* Titrating gene expression using libraries of systematically attenuated CRISPR guide RNAs. *Nat Biotechnol* **38**, 355-364, doi:10.1038/s41587-019-0387-5 (2020).

36 Lin, J. C. *et al.* TROP2 is epigenetically inactivated and modulates IGF-1R signalling in lung adenocarcinoma. *EMBO Mol Med* **4**, 472-485, doi:10.1002/emmm.201200222 (2012).

37 Malumbres, M. CDK4/6 Inhibitors resTORe Therapeutic Sensitivity in HER(2)(+) Breast Cancer. *Cancer Cell* **29**, 243-244, doi:10.1016/j.ccell.2016.02.016 (2016).

38 Alexander, T. B. *et al.* The genetic basis and cell of origin of mixed phenotype acute leukaemia. *Nature* **562**, 373-379, doi:10.1038/s41586-018-0436-0 (2018).

39 Kotrova, M. *et al.* Distinct bilineal leukemia immunophenotypes are not genetically determined. *Blood* **128**, 2263-2266, doi:10.1182/blood-2016-07-725861 (2016).

40 Stoeckius, M. *et al.* Simultaneous epitope and transcriptome measurement in single cells. *Nat Methods* **14**, 865-868, doi:10.1038/nmeth.4380 (2017).

41 Barna, M. *et al.* Suppression of Myc oncogenic activity by ribosomal protein haploinsufficiency. *Nature* **456**, 971-975, doi:10.1038/nature07449 (2008).

42 Kang, J. *et al.* Ribosomal proteins and human diseases: molecular mechanisms and targeted therapy. *Signal Transduct Target Ther* **6**, 323, doi:10.1038/s41392-021-00728-8 (2021).

43 Kampen, K. R., Sulima, S. O., Vereecke, S. & De Keersmaecker, K. Hallmarks of ribosomopathies. *Nucleic Acids Res* **48**, 1013-1028, doi:10.1093/nar/gkz637 (2020).

44 Fancello, L., Kampen, K. R., Hofman, I. J., Verbeeck, J. & De Keersmaecker, K. The ribosomal protein gene RPL5 is a haploinsufficient tumor suppressor in multiple cancer types. *Oncotarget* **8**, 14462-14478, doi:10.18632/oncotarget.14895 (2017).

45 Rao, S. *et al.* Inactivation of ribosomal protein L22 promotes transformation by induction of the stemness factor, Lin28B. *Blood* **120**, 3764-3773, doi:10.1182/blood-2012-03-415349 (2012).

46 De Keersmaecker, K. *et al.* Exome sequencing identifies mutation in CNOT3 and ribosomal genes RPL5 and RPL10 in T-cell acute lymphoblastic leukemia. *Nat Genet* **45**, 186-190, doi:10.1038/ng.2508 (2013).

47 Chen, C. *et al.* Oxidative phosphorylation enhances the leukemogenic capacity and resistance to chemotherapy of B cell acute lymphoblastic leukemia. *Sci Adv* **7**, doi:10.1126/sciadv.abd6280 (2021).

48 Nelson, M. A. *et al.* Intrinsic OXPHOS limitations underlie cellular bioenergetics in leukemia. *Elife* **10**, doi:10.7554/eLife.63104 (2021).

49 Lobrich, M. & Jeggo, P. A. The impact of a negligent G2/M checkpoint on genomic instability and cancer induction. *Nat Rev Cancer* **7**, 861-869, doi:10.1038/nrc2248 (2007).

50 Didier, C. *et al.* G2/M checkpoint stringency is a key parameter in the sensitivity of AML cells to genotoxic stress. *Oncogene* **27**, 3811-3820, doi:10.1038/sj.onc.1211041 (2008).

51 Demaree, B. *et al.* Joint profiling of DNA and proteins in single cells to dissect genotype-phenotype associations in leukemia. *Nat Commun* **12**, 1583, doi:10.1038/s41467-021-21810-3 (2021).

52 Shahi, P., Kim, S. C., Haliburton, J. R., Gartner, Z. J. & Abate, A. R. Abseq: Ultrahigh-throughput single cell protein profiling with droplet microfluidic barcoding. *Sci Rep* **7**, 44447, doi:10.1038/srep44447 (2017).

53 Gaiti, F. *et al.* Epigenetic evolution and lineage histories of chronic lymphocytic leukaemia. *Nature* **569**, 576-580, doi:10.1038/s41586-019-1198-z (2019).

54 Ma, S. *et al.* Chromatin Potential Identified by Shared Single-Cell Profiling of RNA and Chromatin. *Cell* **183**, 1103-1116 e1120, doi:10.1016/j.cell.2020.09.056 (2020).

55 Hao, Y. *et al.* Dictionary learning for integrative, multimodal, and scalable single-cell analysis. *bioRxiv*, 2022.2002.2024.481684, doi:10.1101/2022.02.24.481684 (2022).

56 Ghazanfar, S., Guibentif, C. & Marioni, J. C. StabMap: Mosaic single cell data integration using non-overlapping features. *bioRxiv*, 2022.2002.2024.481823, doi:10.1101/2022.02.24.481823 (2022).

57 Hao, Y. *et al.* Integrated analysis of multimodal single-cell data. *Cell* **184**, 3573-3587 e3529, doi:10.1016/j.cell.2021.04.048 (2021).

58 Squair, J. W. *et al.* Confronting false discoveries in single-cell differential expression. *Nat Commun* **12**, 5692, doi:10.1038/s41467-021-25960-2 (2021).

59 Hughes, T. K. *et al.* Second-Strand Synthesis-Based Massively Parallel scRNA-Seq Reveals Cellular States and Molecular Features of Human Inflammatory Skin Pathologies. *Immunity* **53**, 878-894 e877, doi:10.1016/j.immuni.2020.09.015 (2020).

60 De Rop, F. V. *et al.* Hydrop enables droplet-based single-cell ATAC-seq and single-cell RNA-seq using dissolvable hydrogel beads. *Elife* **11**, doi:10.7554/eLife.73971 (2022).

61 Mejstrikova, E. *et al.* Prognosis of children with mixed phenotype acute leukemia treated on the basis of consistent immunophenotypic criteria. *Haematologica* **95**, 928-935, doi:10.3324/haematol.2009.014506 (2010).

62 Takahashi, K. *et al.* Integrative genomic analysis of adult mixed phenotype acute leukemia delineates lineage associated molecular subtypes. *Nat Commun* **9**, 2670, doi:10.1038/s41467-018-04924-z (2018).

63 Ebright, R. Y. *et al.* Deregulation of ribosomal protein expression and translation promotes breast cancer metastasis. *Science* **367**, 1468-1473, doi:10.1126/science.aay0939 (2020).

64 Khot, A. *et al.* First-in-Human RNA Polymerase I Transcription Inhibitor CX-5461 in Patients with Advanced Hematologic Cancers: Results of a Phase I Dose-Escalation Study. *Cancer Discov* **9**, 1036-1049, doi:10.1158/2159-8290.CD-18-1455 (2019).

65 DeJournette, C. J. *et al.* Creating biocompatible oil-water interfaces without synthesis: direct interactions between primary amines and carboxylated perfluorocarbon surfactants. *Analytical Chemistry* **85**, 10556-10564, doi:10.1021/ac4026048 (2013).

66 Labarge, M. A., Garbe, J. C. & Stampfer, M. R. Processing of human reduction mammoplasty and mastectomy tissues for cell culture. *J Vis Exp*, doi:10.3791/50011 (2013).

67 Patro, R., Duggal, G., Love, M. I., Irizarry, R. A. & Kingsford, C. Salmon provides fast and bias-aware quantification of transcript expression. *Nat Methods* **14**, 417-419, doi:10.1038/nmeth.4197 (2017).

68 Srivastava, A., Malik, L., Smith, T., Sudbery, I. & Patro, R. Alevin efficiently estimates accurate gene abundances from dscRNA-seq data. *Genome Biol* **20**, 65, doi:10.1186/s13059-019-1670-y (2019).

69 Lun, A. T. L. *et al.* EmptyDrops: distinguishing cells from empty droplets in droplet-based single-cell RNA sequencing data. *Genome Biol* **20**, 63, doi:10.1186/s13059-019-1662-y (2019).

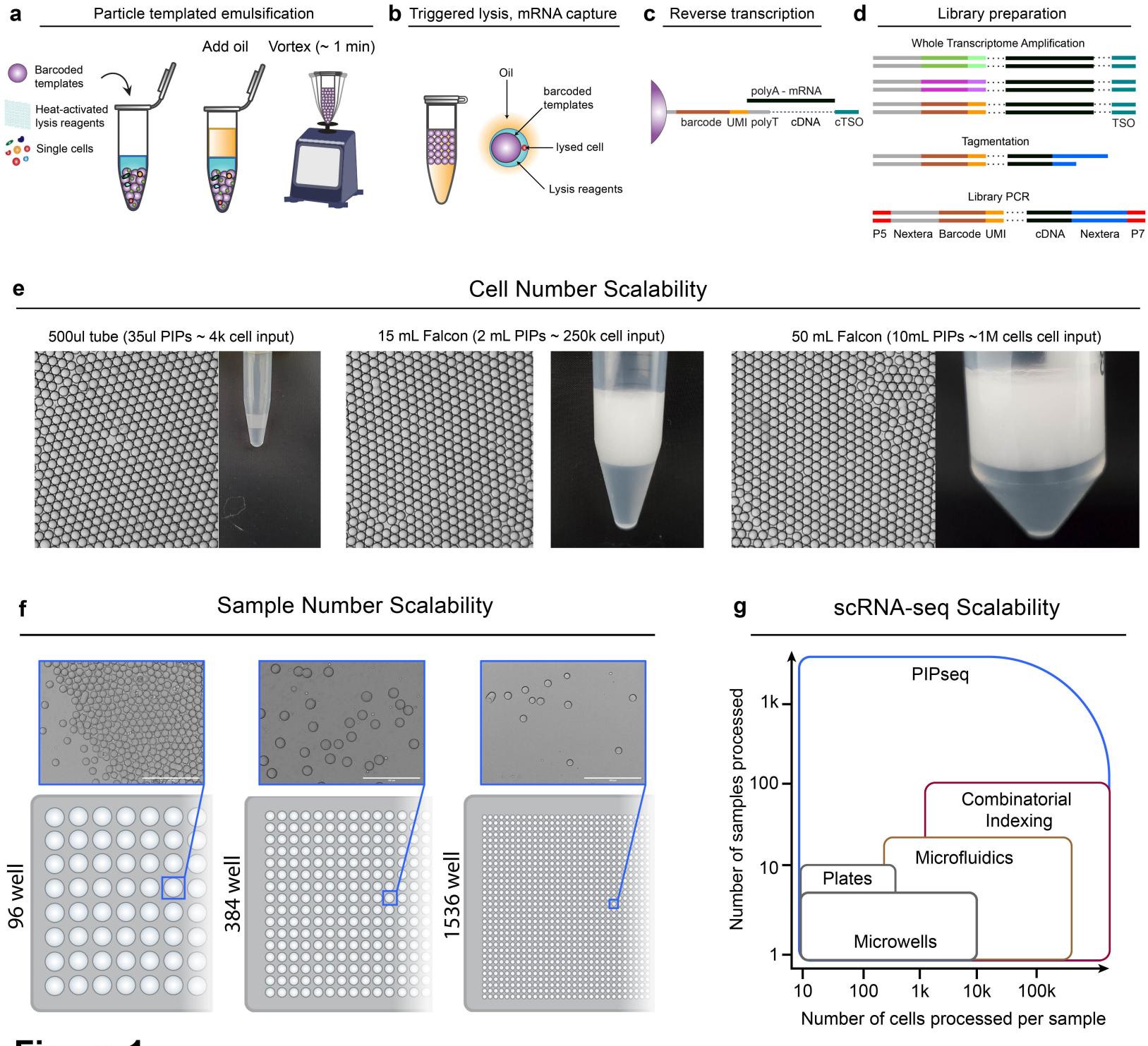
a
Particle templated emulsification
Barcoded templates
Heat-activated lysis reagents
Single cells
Add oil
Vortex (~ 1 min)
b
Triggered lysis, mRNA capture
Oil
barcoded templates
lysed cell
Lysis reagents
c
Reverse transcription
polyA - mRNA
barcode UMI polyT cDNA cTSO
d
Library preparation
Whole Transcriptome Amplification
TSO
Tagmentation
Library PCR
P5 Nextera Barcode UMI cDNA Nextera P7
e
Cell Number Scalability
500ul tube (35ul PIPs ~ 4k cell input)
15 mL Falcon (2 mL PIPs ~ 250k cell input)
50 mL Falcon (10mL PIPs ~1M cells cell input)
f
Sample Number Scalability
96 well
384 well
1536 well
g
scRNA-seq Scalability
PIPseq
Combinatorial Indexing
Microfluidics
Plates
Microwells
Number of samples processed
1k
100
10
1
10
100
1k
10k
100k
Number of cells processed per sample

Figure 1

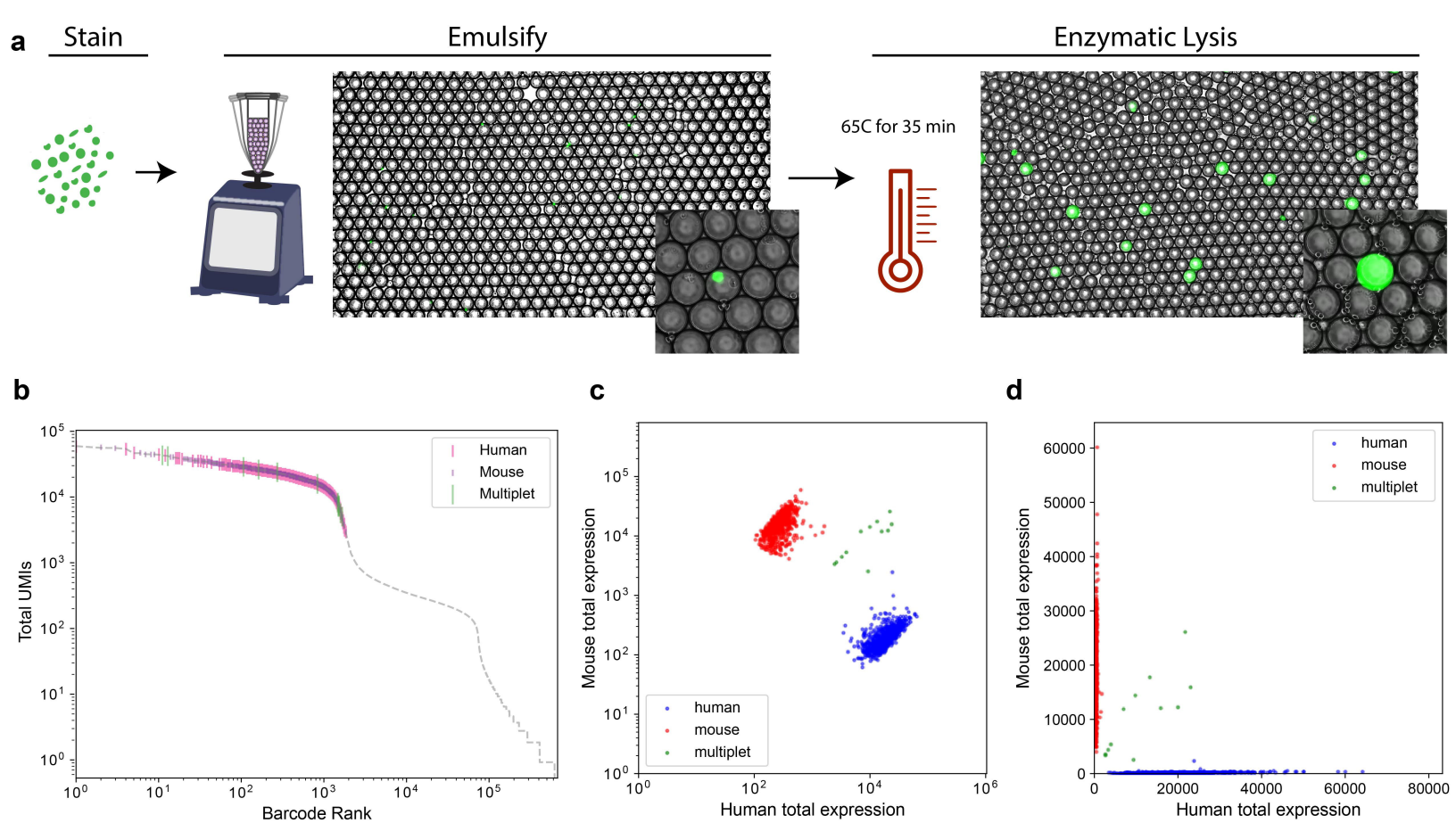
a
Stain
Emulsify
Enzymatic Lysis
65C for 35 min
b
Total UMIs
Barcode Rank
Human
Mouse
Multiplet
c
Mouse total expression
Human total expression
human
mouse
multiplet
d
Mouse total expression
Human total expression
human
mouse
multiplet

Figure 2

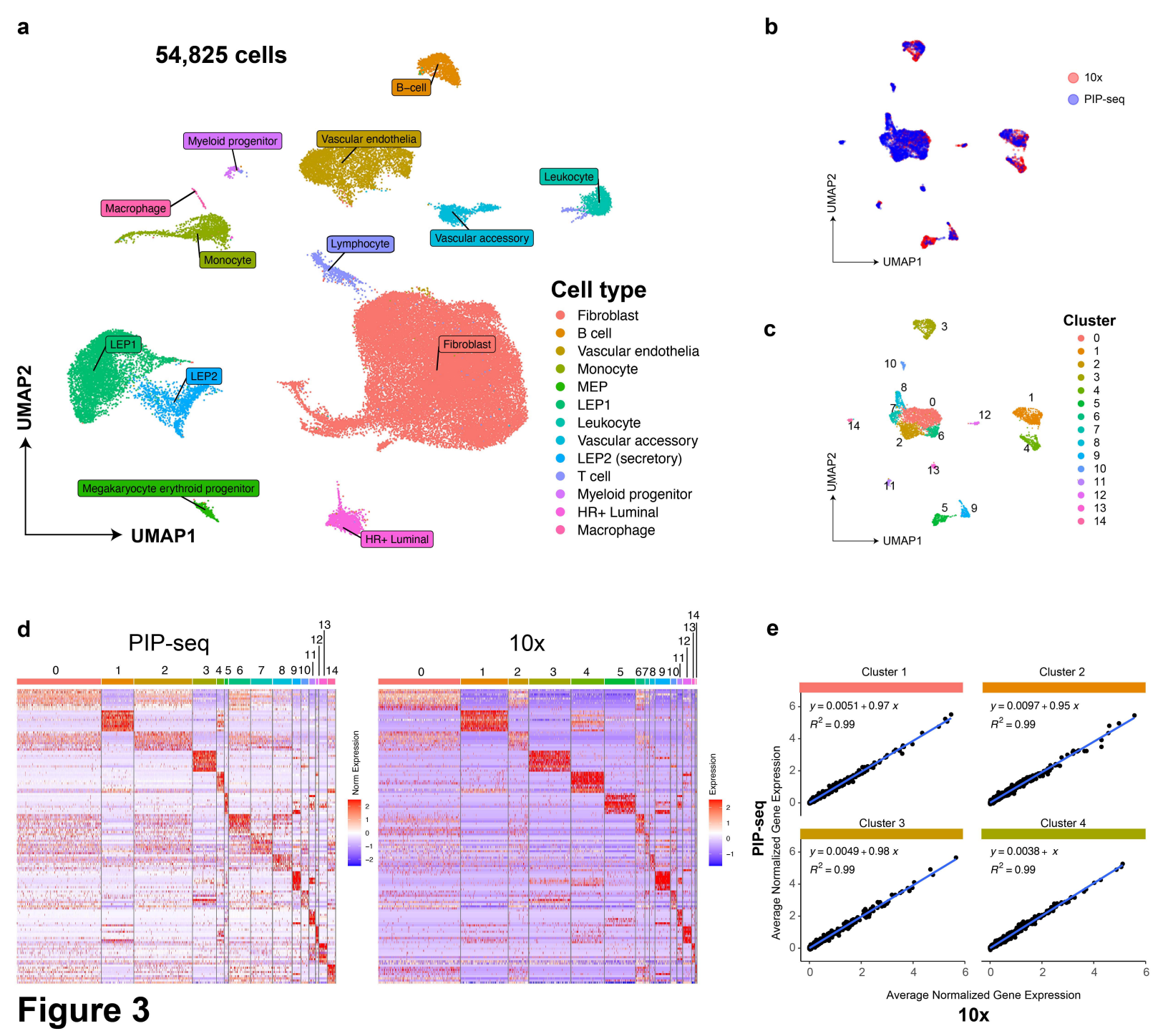
a
54,825 cells
B–cell
Myeloid progenitor
Vascular endothelia
Leukocyte
Macrophage
Vascular accessory
Monocyte
Lymphocyte
Fibroblast
LEP1
LEP2
Megakaryocyte erythroid progenitor
HR+ Luminal
UMAP2
UMAP1
Cell type
Fibroblast
B cell
Vascular endothelia
Monocyte
MEP
LEP1
Leukocyte
Vascular accessory
LEP2 (secretory)
T cell
Myeloid progenitor
HR+ Luminal
Macrophage
b
10x
PIP-seq
UMAP2
UMAP1
c
Cluster
UMAP2
UMAP1
d
PIP-seq
10x
Norm Expression
Expression
e
Cluster 1
Cluster 2
Cluster 3
Cluster 4
y = 0.0051 + 0.97 x
R2 = 0.99
y = 0.0097 + 0.95 x
R2 = 0.99
y = 0.0049 + 0.98 x
R2 = 0.99
y = 0.0038 + x
R2 = 0.99
PIP-seq
Average Normalized Gene Expression
Average Normalized Gene Expression
10x

Figure 3

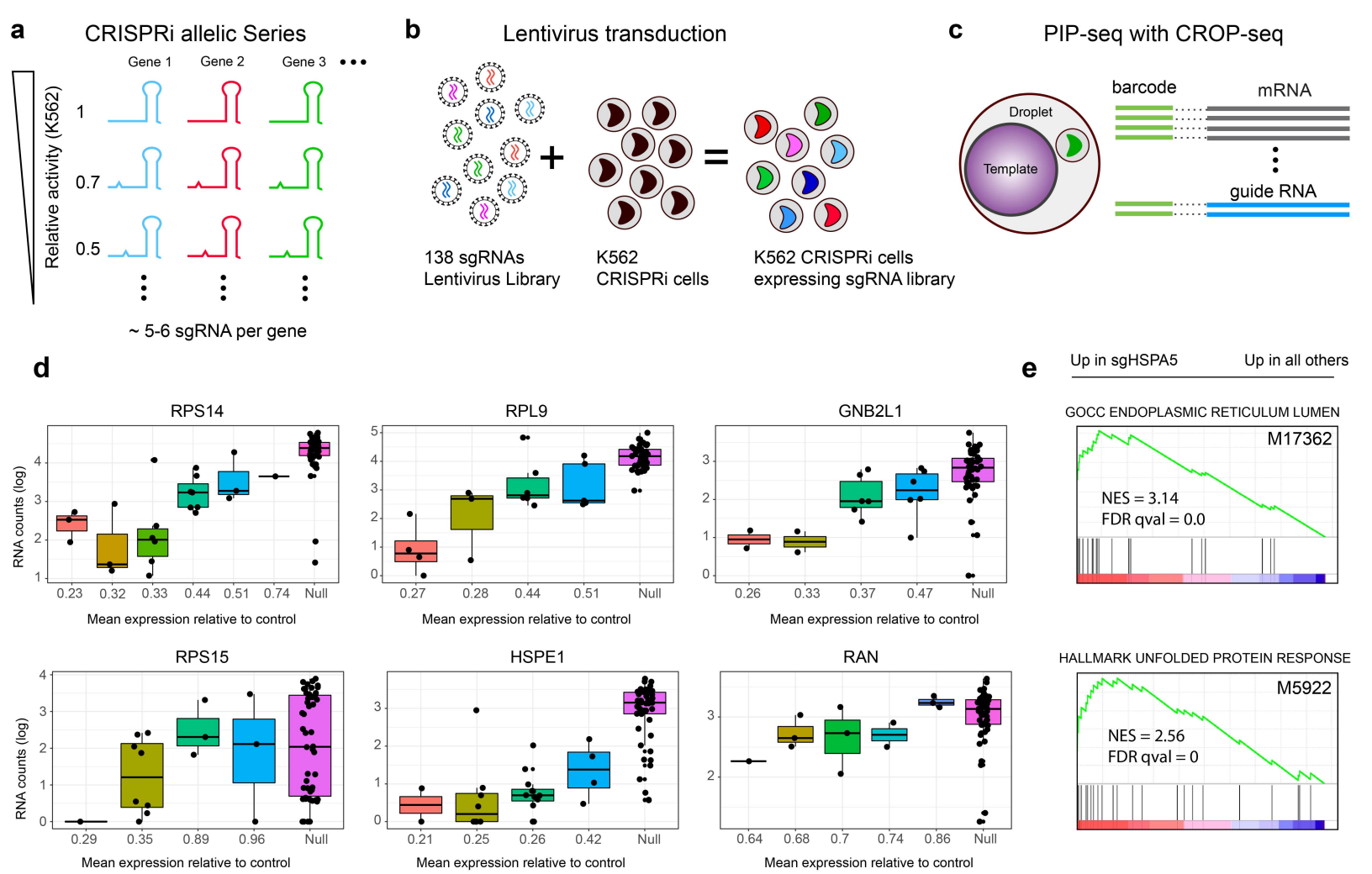
a
CRISPRi allelic Series
Gene 1
Gene 2
Gene 3
Relative activity (K562)
1
0.7
0.5
~ 5-6 sgRNA per gene
b
Lentivirus transduction
138 sgRNAs
Lentivirus Library
K562
CRISPRi cells
K562 CRISPRi cells
expressing sgRNA library
c
PIP-seq with CROP-seq
Droplet
Template
barcode
mRNA
guide RNA
d
RPS14
RPL9
GNB2L1
RPS15
HSPE1
RAN
RNA counts (log)
Mean expression relative to control
e
Up in sgHSPA5
Up in all others
GOCC ENDOPLASMIC RETICULUM LUMEN
M17362
NES = 3.14
FDR qval = 0.0
HALLMARK UNFOLDED PROTEIN RESPONSE
M5922
NES = 2.56
FDR qval = 0

Figure 4

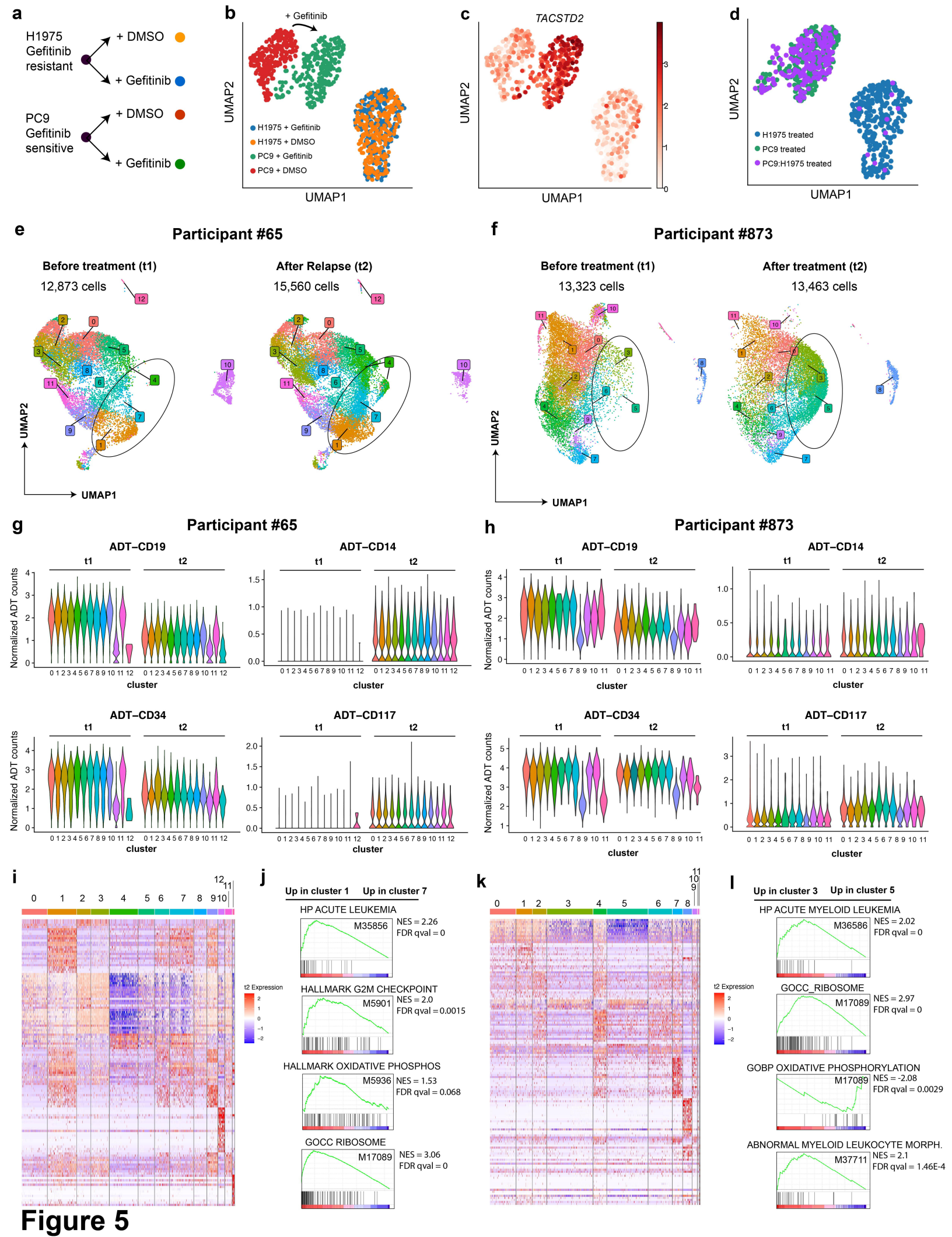
a
H1975 Gefitinib resistant
+ DMSO
+ Gefitinib
PC9 Gefitinib sensitive
+ DMSO
+ Gefitinib
b
+ Gefitinib
UMAP2
UMAP1
H1975 + Gefitinib
H1975 + DMSO
PC9 + Gefitinib
PC9 + DMSO
c
TACSTD2
UMAP2
UMAP1
d
UMAP2
UMAP1
H1975 treated
PC9 treated
PC9:H1975 treated
e
Participant #65
Before treatment (t1)
12,873 cells
After Relapse (t2)
15,560 cells
UMAP2
UMAP1
f
Participant #873
Before treatment (t1)
13,323 cells
After treatment (t2)
13,463 cells
UMAP2
UMAP1
g
Participant #65
ADT−CD19
ADT−CD14
ADT−CD34
ADT−CD117
t1
t2
Normalized ADT counts
cluster
h
Participant #873
ADT−CD19
ADT−CD14
ADT−CD34
ADT−CD117
t1
t2
Normalized ADT counts
cluster
i
t2 Expression
j
Up in cluster 1
Up in cluster 7
HP ACUTE LEUKEMIA
M35856
NES = 2.26
FDR qval = 0
HALLMARK G2M CHECKPOINT
M5901
NES = 2.0
FDR qval = 0.0015
HALLMARK OXIDATIVE PHOSPHOS
M5936
NES = 1.53
FDR qval = 0.068
GOCC RIBOSOME
M17089
NES = 3.06
FDR qval = 0
k
t2 Expression
l
Up in cluster 3
Up in cluster 5
HP ACUTE MYELOID LEUKEMIA
M36586
NES = 2.02
FDR qval = 0
GOCC_RIBOSOME
M17089
NES = 2.97
FDR qval = 0
GOBP OXIDATIVE PHOSPHORYLATION
M17089
NES = -2.08
FDR qval = 0.0029
ABNORMAL MYELOID LEUKOCYTE MORPH.
M37711
NES = 2.1
FDR qval = 1.46E-4

Figure 5

a

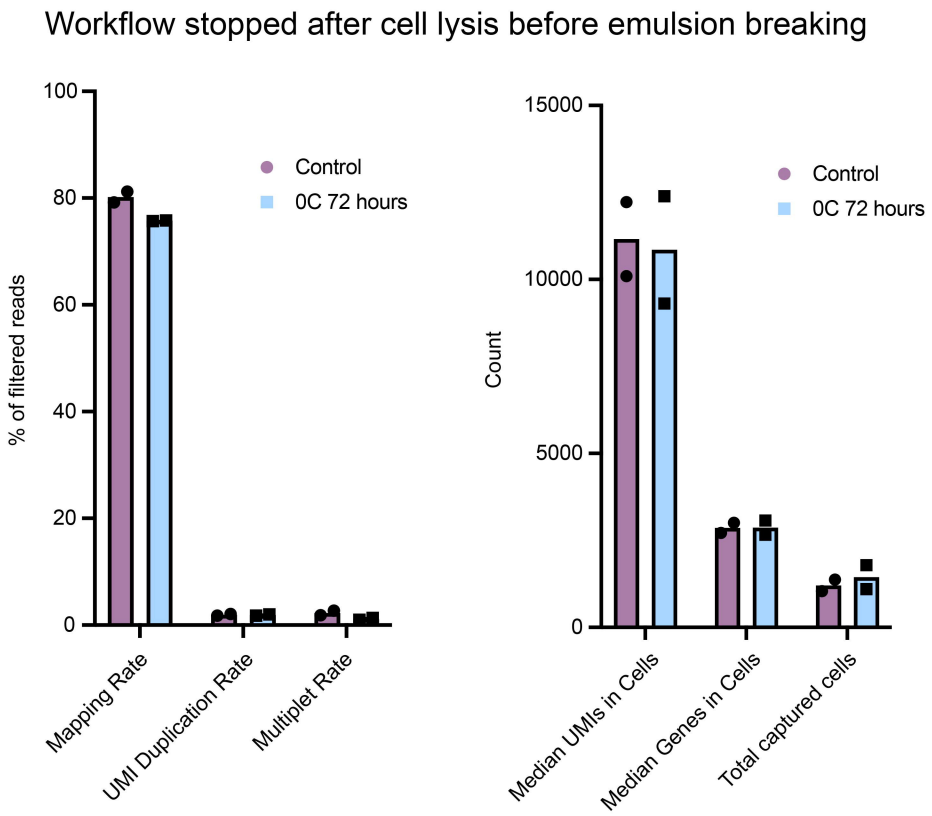

b

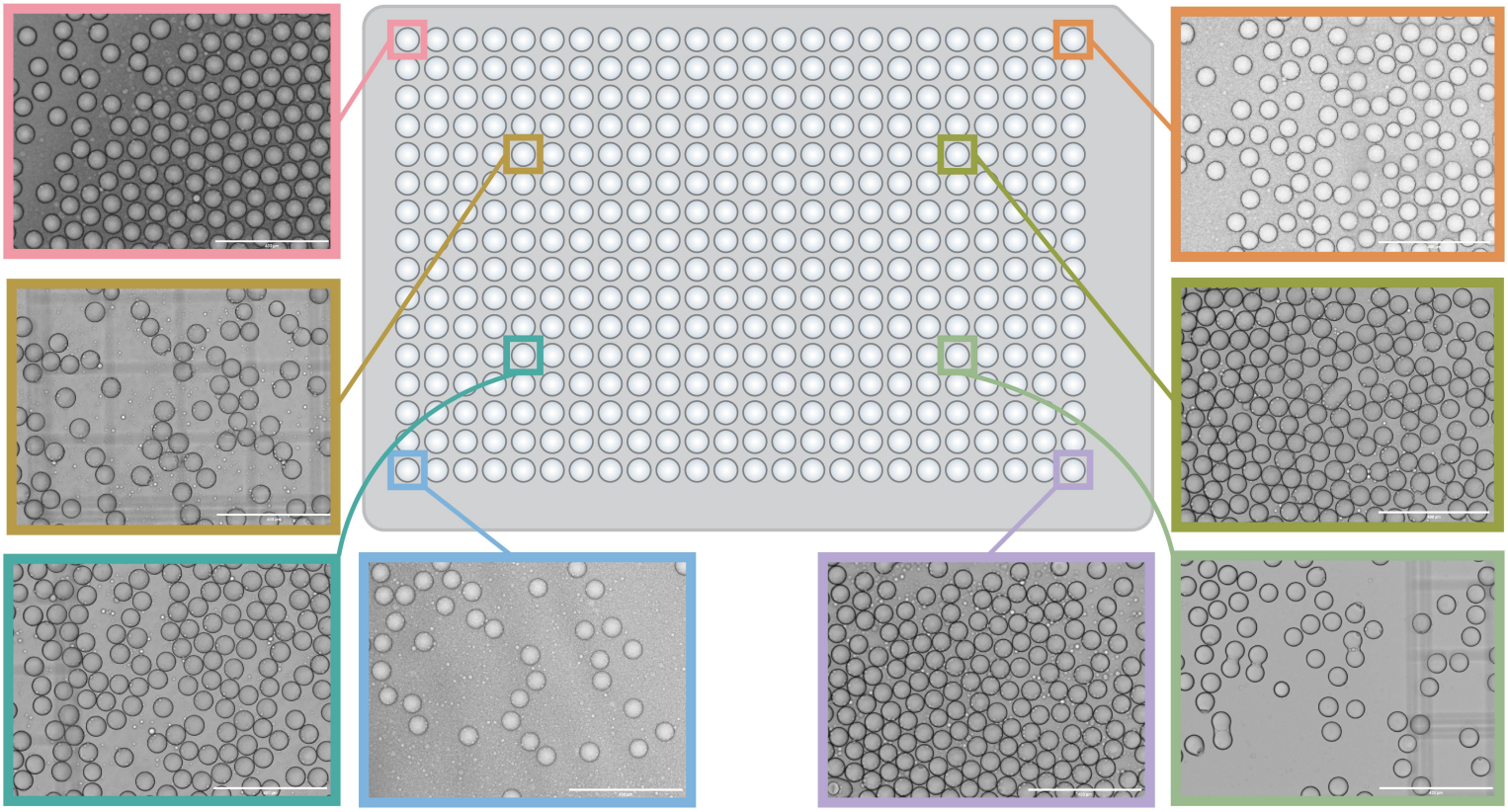

Extended data Figure 1

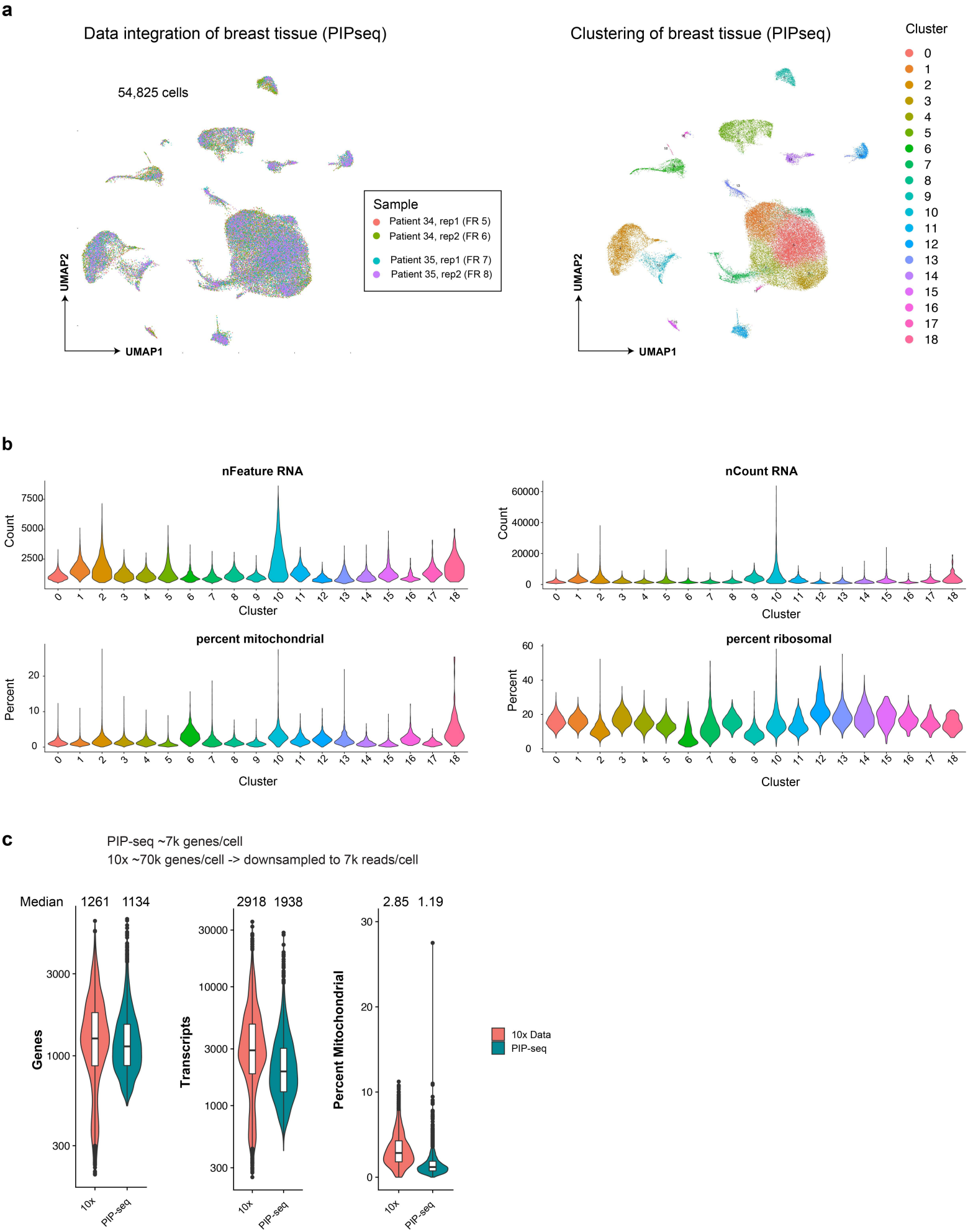

Extended data Figure 2

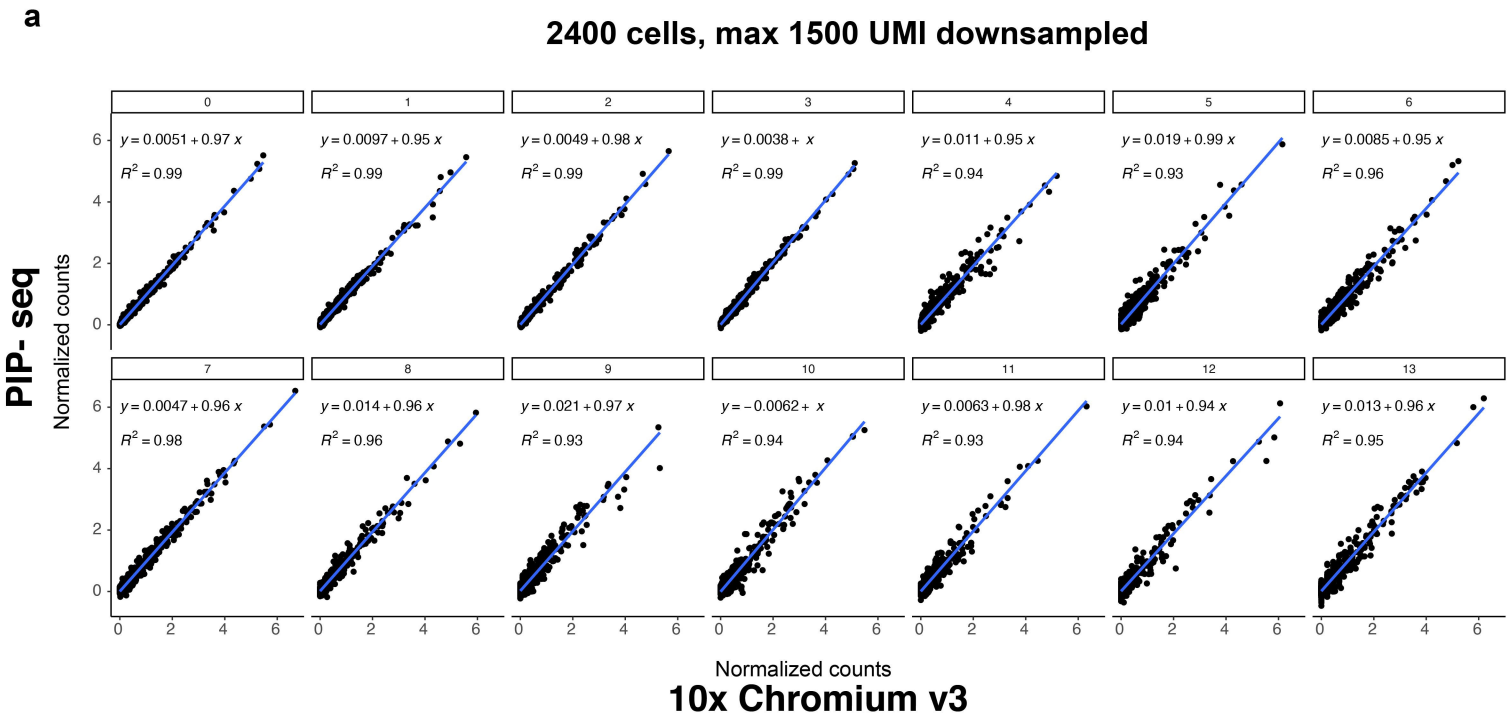

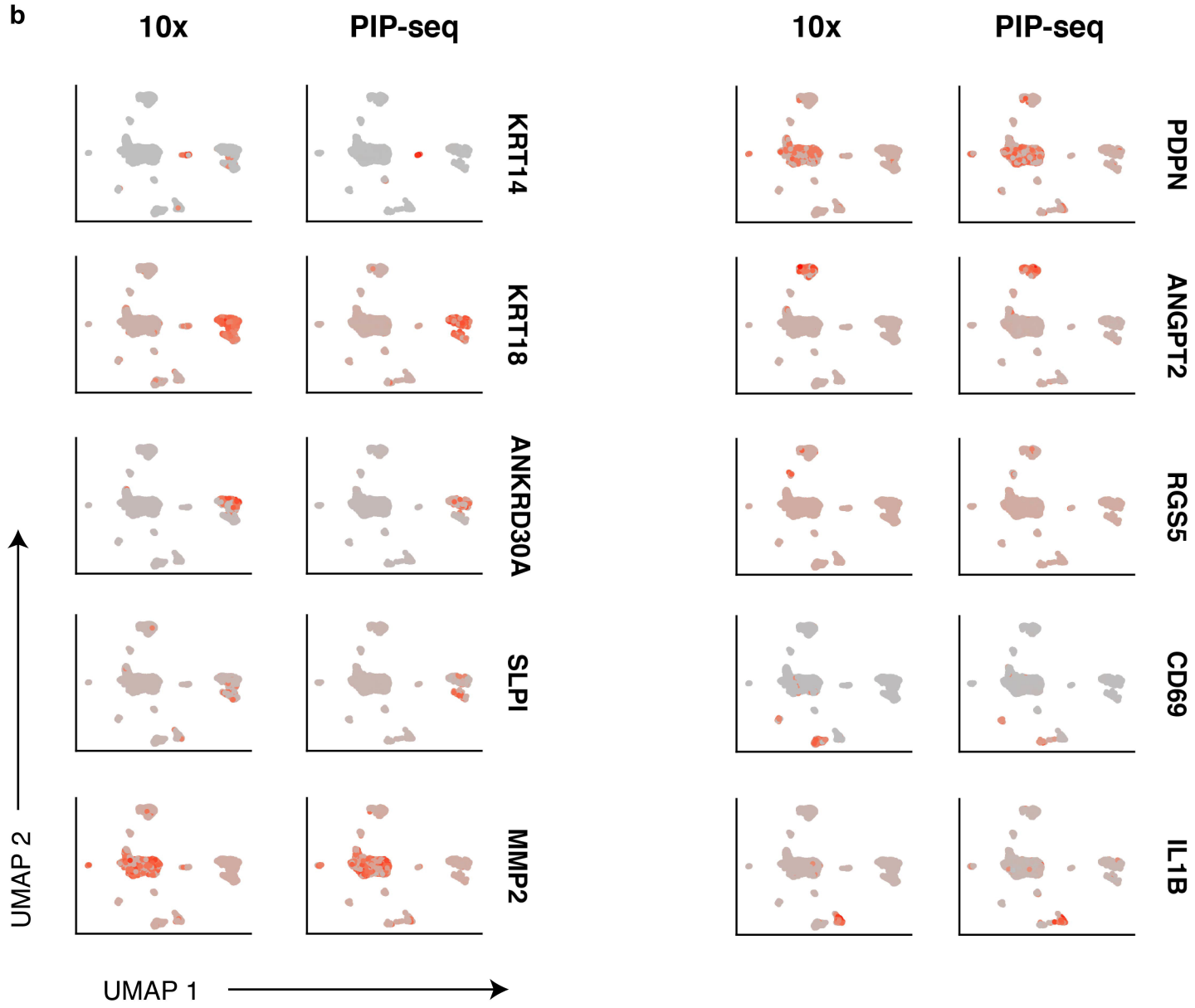

Extended data Figure 3

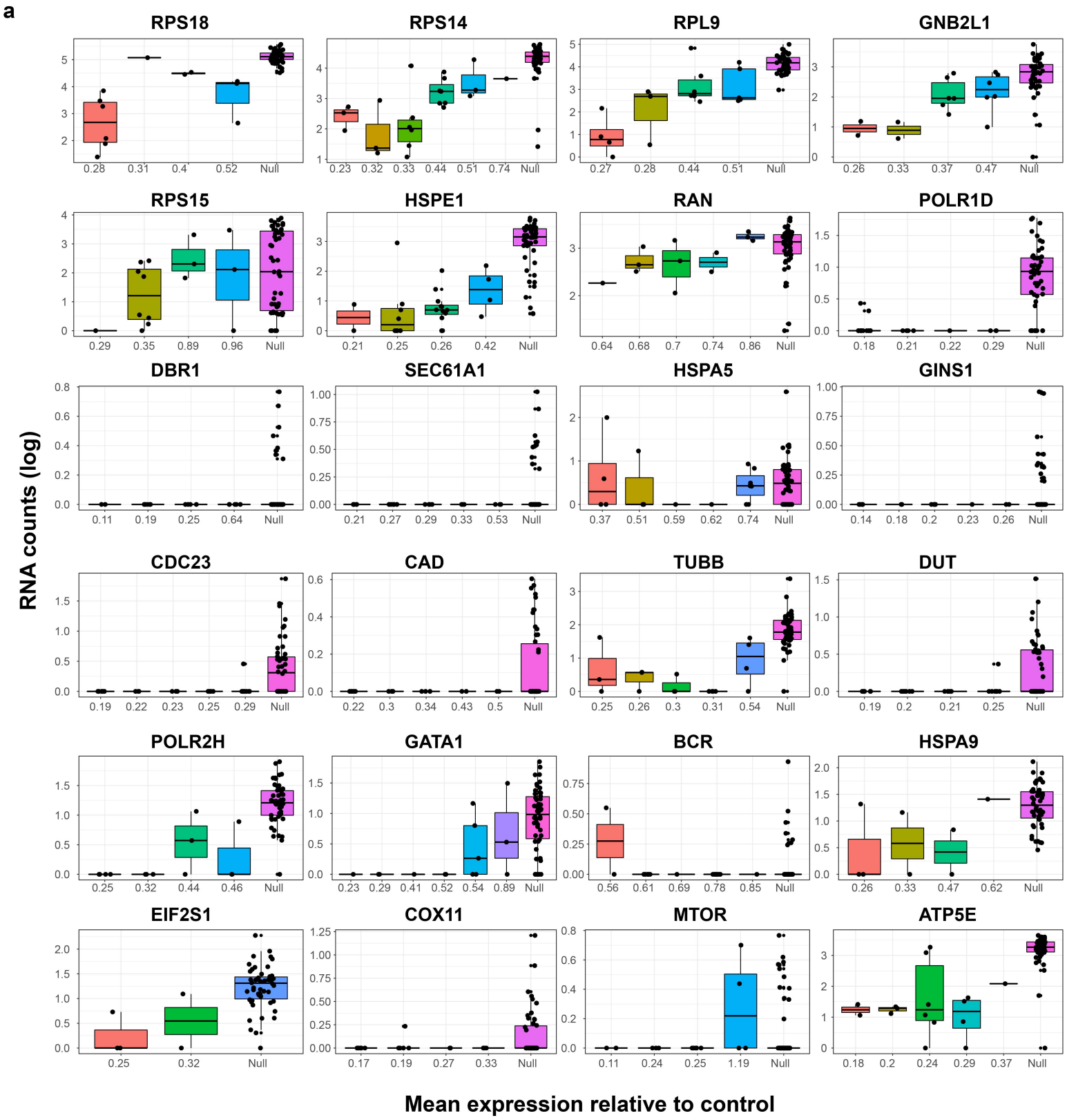

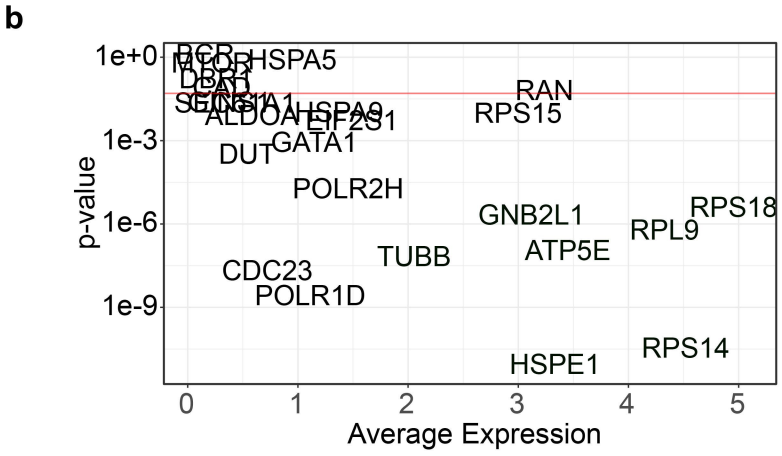

Extended data Figure 4

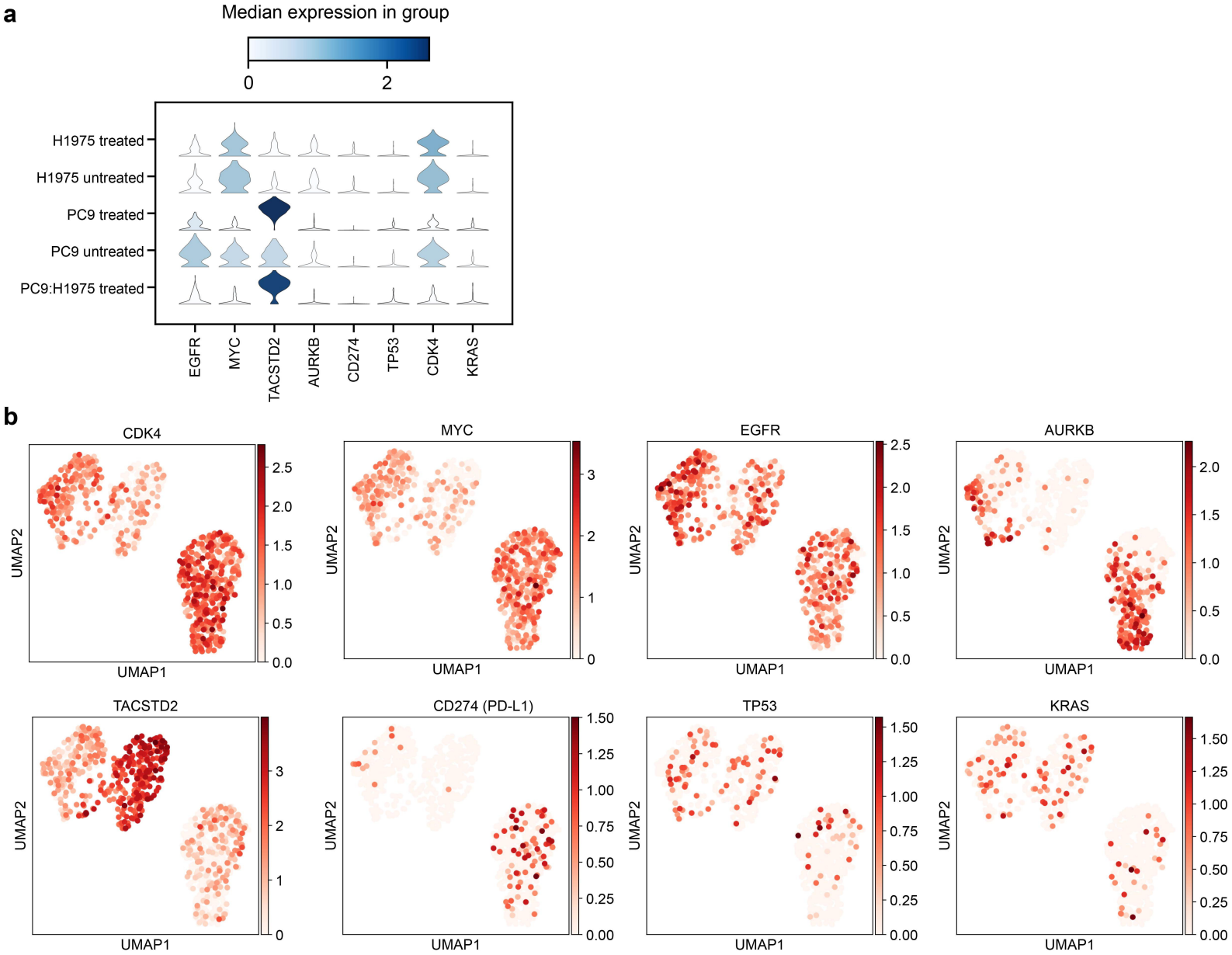

Extended data Figure 5

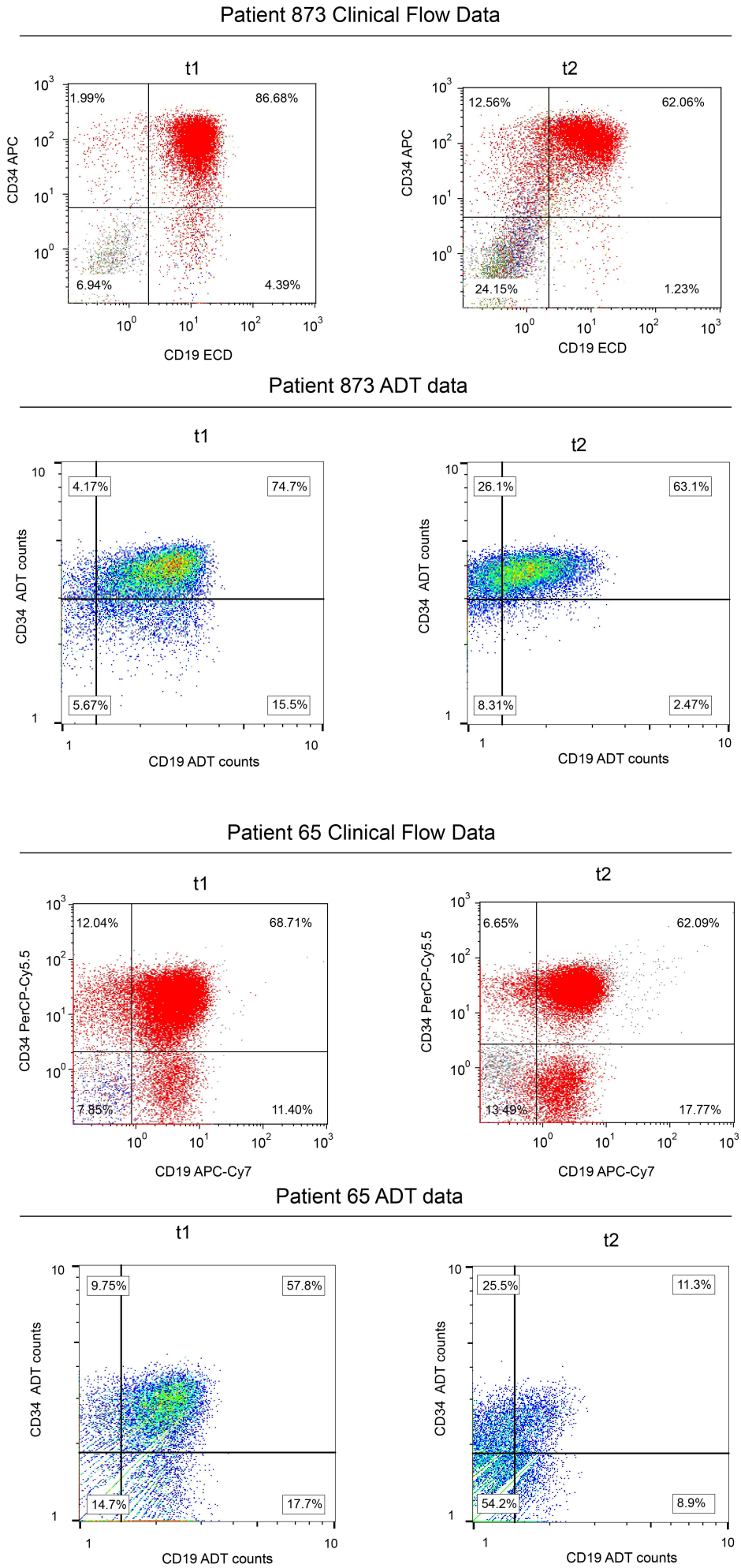

Extended data Figure 6

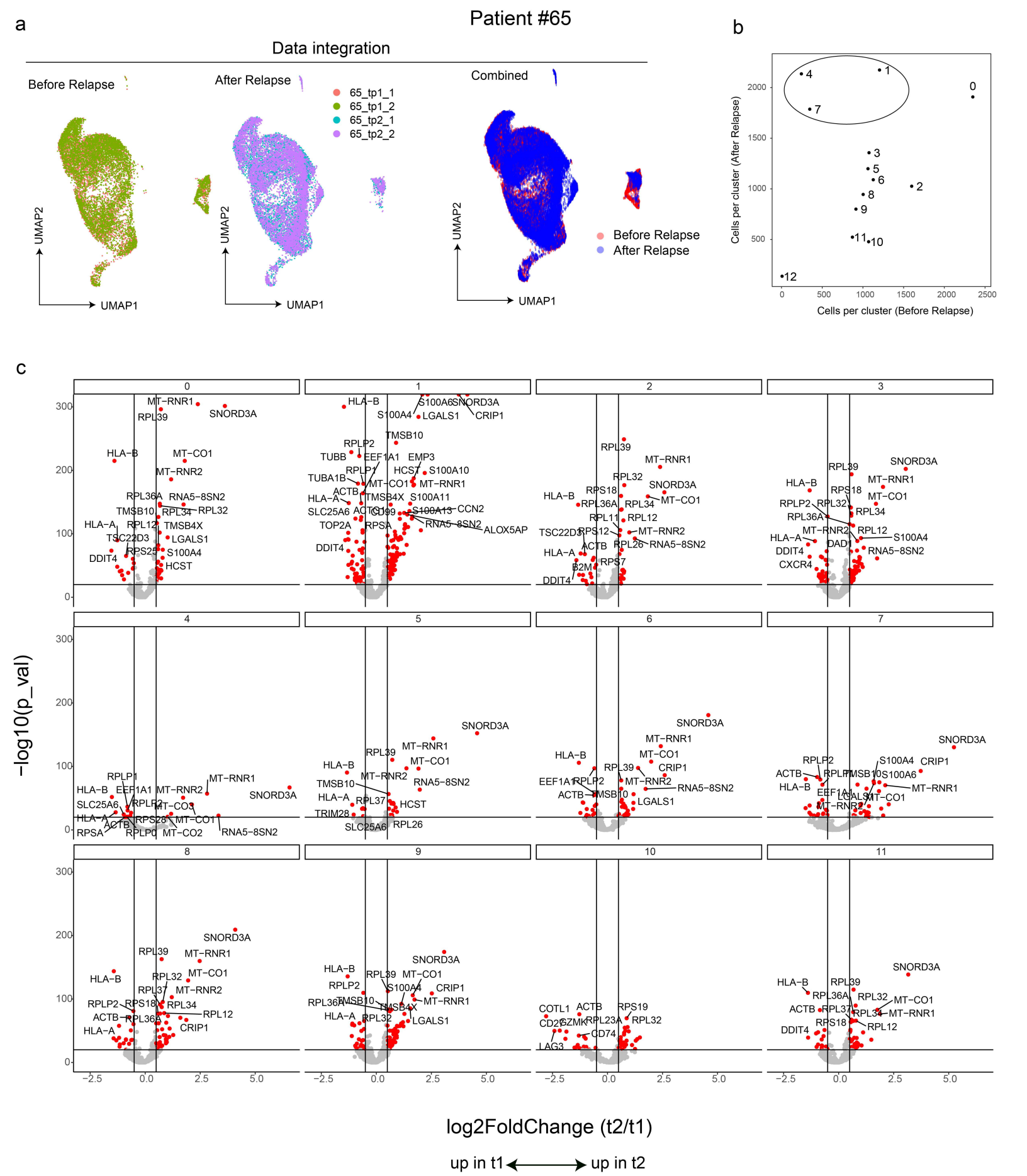

Extended data Figure 7

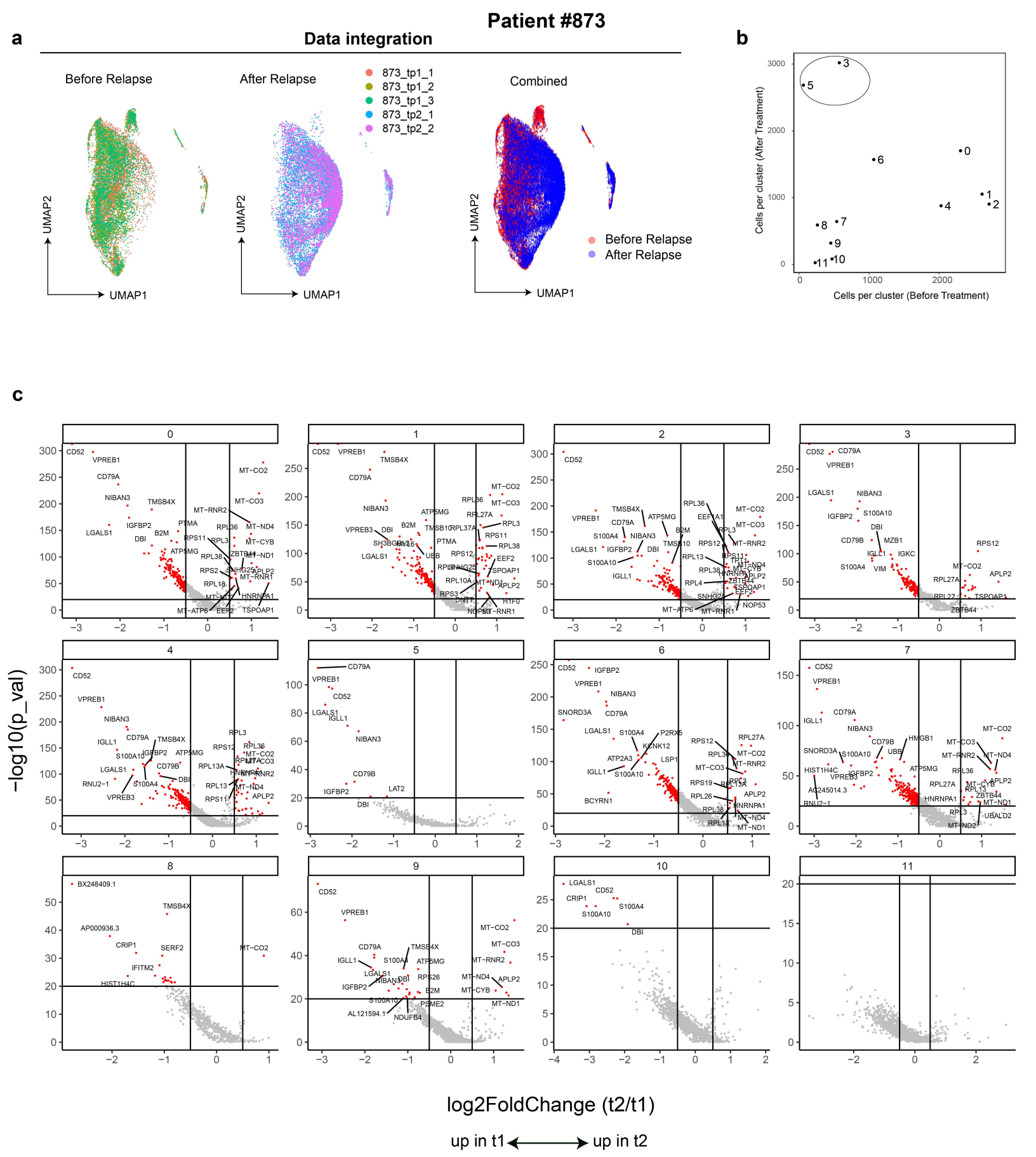

Extended data Figure 8